POLITECNICO DI TORINO

Collegio di Ingegneria Chimica e dei Materiali

Master of Science Course in Materials Engineering for Industry 4.0

Master of Science Thesis

Development of a hybrid cryogenic cooling concept for a turning tool with internal cooling via liquid nitrogen



Tutors

Prof. Daniele Ugues

Prof. Milena Salvo

Candidate



Settembre 2025

Erasmus Mundus Joint Master in Manufacturing 4.0 by intElligent and susTAinable technologies



MASTER's Degree Thesis

Development of a hybrid cryogenic cooling concept for a turning tool with internal cooling via liquid nitrogen

Supervisors

Prof. Dr.-Ing. Martin DIX

Dr.-Ing. Matthias REHM

Prof. Cedric COURBON

Prof. Daniele UGUES

Candidate

Guta Asrat DURESSA

September 2025











Univerza v Ljubljani



Abstract

This thesis presents the design, simulation-based evaluation, and parametric analysis of a turning tool with an integrated internal liquid nitrogen (LN_2) cooling chamber for cryogenic machining applications. The primary objective is to provide a foundational design concept and demonstrate structural stability for the tool, which features an integrated cooling chamber, to guide the future development of an internally cooled cutting tool.

Simulation variants were designed by design of experiment using CCD full factorial RSM. A structured DOE incorporates three continuous factors (heat transfer coefficient, tip temperature, and atmospheric temperature), and two categorical factors (insulation method and chamber size). 80 simulation matrices were developed and analysed under steady state thermal analysis, and the resulting temperature loads are applied as a boundary condition in structural analysis, which also considered machining forces representative of hard turning.

Results showed superior thermal performance under chamber coating insulation by localizing cooling around the cutting insert. The maximum Von Mises stress in this configuration is reduced by over 63% compared to dry conditions and 59.5% compared to the configuration with an insulation pad between the tool head and shank.

The parametric analysis using RSM confirmed that HTC, tip temperature, insulation method, and chamber size influence the tool performance, with insulation method as the most influential factor for the tool design. These findings demonstrate that thermal loadings and structural stability are effective under the integrated LN_2 cooling with a targeted insulation, providing a starting point for further optimization, experimental validation, and industrial implementation.

Keywords: Cryogenic cooling, Thermal analysis, Structural analysis, Response surface method, Turning tool, Tool head design, Integrated cooling chamber, LN₂ cooling.

Acknowledgments

First and foremost, I would like to thank God, who is always by my side whenever I need him the most. His guidance has been a source of my strength and comfort in every situation throughout my journey.

I am truly grateful to everyone who supported me during this journey. This thesis would not have been accomplished without their help. My deepest appreciation goes to my supervisors: Mr. Steffen Brier, Dr.-Ing. Matthias Rehm, and Prof. Dr. Ing.-Martin Dix from the Technical University of Chemnitz (TUC) for their constant support, valuable feedback, and guidance, which were crucial to the success of this research. Prof. Cedric Courbon from ENISE, Prof. Milena Salvo, and Prof. Daniele Ugues from POLITO; their guidance in all directions was valuable.

Beyond my supervisors, I would like to express my sincere gratitude to meta 4.0 community, especially Dr. Aurelie Brayet, for always being available and providing administrative procedural support.

I am also grateful to Dr.-Ing. Joachim Regel for his technical support during my thesis, and Prof. Dr.-Ing. Stephen Odenwald for his guidance in research writing and support in all directions at TUC.

I would also like to acknowledge the professorship of Production Systems and Processes, as well as the entire professorial community, for their welcoming environment and support. In particular, I am very grateful to Ms. Katja Klöden for her kind and reliable administrative assistance throughout my work.

Finally, I want to acknowledge my family and friends, whose love, prayers, and support kept me going and motivated me to finish this work.

Table of contents

Abstract	I
Acknowledgments	II
Table of contents	III
List of figures	v
List of tables	VII
Nomenclature	VIII
Chapter 1 Introduction and background	1
1.1. Background	1
1.2. Comparison of cooling strategies	2
1.3. Cryogenic application in machining	3
1.4. Thesis structure	4
Chapter 2 Literature review	5
2.1. Cryogenic properties	6
2.2. Surface heat transfer coefficients in cryogeni	c cooling 7
2.3. Cooling approaches using cryogenic coolants	9
2.4. Tool construction	11
2.5. Task specification	14
2.5.1. Problem statement	14
2.6. Objective of the study	15
2.6.1. Specific objectives	15
2.7. Scope of the study	16
Chapter 3 Methodology	17
3.1. Concept generation and tool modelling	17
3.2. Simulation planning	19

3.3. Simu	lation study	21
3.3.1.	Material selection and assignment	21
3.3.2.	Meshing strategy	25
3.3.3.	Boundary conditions	28
3.3.4.	Simulation types	29
Chapter 4	Results and discussion	32
4.1. Simu	lation results	32
4.1.1.	Thermal analysis results	32
4.1.2.	Structural analysis results	40
4.1.3.	Effect of the tool head material on the structural stability	44
4.2. Parar	netric analysis of key factors	45
4.2.1.	Model adequacy and ANOVA results	45
4.2.2.	Response surface and interaction plots	49
Chapter 5	Conclusion and future work	53
5.1. Conc	lusion	53
5.2. Futur	re work	55
Appendix	A	56
Appendix	В	60
Appendix	С	61
Bibliograp	ohy	63

List of figures

Figure 1.1 : Cryogenic machining and processing application [11].

3

Figure 2.1: Illustration of hybrid machining used by Z.Y. Wang [36].
Figure 2.2: Internal micro-channel cooled tool [38].
Figure $3.1:a$) Turning tool assembly with integrated insulation pad, b) with expansion
chamber coating, c) tool head with larger expansion chamber, d) tool head with small
expansion chamber.
Figure 3.2: Top 21 candidate materials a) fracture toughness-yield strength graph b
yield strength-density graph.
Figure 3.3: Top 9 candidate materials for the tool head after performance index
application.
Figure 3.4 : Meshing strategies for variant 1 with chamber coating a) assembled part b
tool head with internal chamber coating c) sectioned part of the assembly d) cutting
insert e) insert support.
$Figure \ 3.5: meshing \ strategies \ of \ variant \ 2 \ with \ insulation \ pad \ between \ head \ and \ shank \$
a) tool assembly b) tool head c) sectioned part of the assembly d)insert support e) cutting a section of the assembly d s
insert. 27
Figure 3.6 : Boundary conditions of the model.
$Figure\ 4.1: Temperature\ distribution\ results\ from\ steady\ state\ thermal\ simulation\ of\ thermal\ simulation\ simulation\ of\ thermal\ simulation\ simulation\ of\ simulation\ simul$
internally cooled turning tool: a) cutting tool under cryogenic cooling conditions, b
temperature distribution of the tool under dry conditions, c) sectional view under
cryogenic cooling, d) sectional view under dry conditions.
Figure $4.2:$ Temperature distribution along the diagonal path, a) cryogenically cooled
tool, b) dry machining. c) graph for the temperature distribution of the dry and
cryogenically cooled tool. 34
$Figure\ 4.3: Temperature\ distribution\ along\ the\ tool\ holder\ length\ for\ the\ model\ with\ any property of the propert$
insulation pad between the tool head and shank. A) cooled by LN_2 , b) dry machining. 36
$Figure\ 4.4: Temperature\ distribution\ along\ the\ diagonal\ path\ for\ the\ configuration\ with$
an insulation pad between head and shank, a) cryogenically cooled tool, b) dry
$machining.\ c)\ graph\ for\ the\ temperature\ distribution\ of\ the\ dry\ and\ cryogenically\ cooled$
tool.

$Figure\ 4.5: Temperature\ distribution\ along\ the\ diagonal\ path\ through\ the\ cutting\ insertion and the path\ through\ the\ cutting\ insertion and\ the\ diagonal\ path\ through\ the\ cutting\ insertion and\ the\ diagonal\ path\ through\ the\ cutting\ insertion and\ the\ path\ through\ throu$	er
at different time intervals.	38
Figure 4.6 : Time evolution of maximum, minimum, and average temperatures.	39
Figure 4.7: Temperature distribution along the diagonal path of the tool for different	ent
configurations.	39
Figure 4.8: Stress distribution through the tool under cryogenic cooling conditions	foi
the tool variant with insulation coating in the LN ₂ chamber.	40
Figure 4.9: stress distribution through the tool under cryogenic cooling conditions	foi
the tool variant with an insulation pad between the tool head and shank.	41
Figure 4.10: Maximum Von Mises stress on the tool under different conditions.	42
Figure $4.11:$ Total deformation throughout the tool a) tool with insulation coating in t	the
chamber, b) variant with an insulation pad between the tool head and shank.	43
Figure 4.12: a) maximum stress for different tool head materials under identi	ca
conditions, b) maximum deformation for different tool head materials under identi-	ca
conditions.	44
Figure 4.13: Model summary a) maximum stress model, b) maximum deformati	or
model.	45
Figure 4.14: Pareto chart a) maximum stress, b) maximum deformation models.	49
Figure 4.15: Response surface and interaction plots for maximum deformation of varia	ant
model 1.	50
Figure 4.16: Response surface and interaction plots for maximum stress of varia	ant
model 1.	51
Figure 4.17: Response surface and interaction plot for maximum deformation of varia	ant
model 2.	52
$Figure\ 4.18: Response\ surface\ and\ interaction\ plot\ for\ maximum\ stress\ of\ variant\ models and\ stress\ of\ variant\ models and\ stress\ of\ variant\ models and\ stress\ of\ variant\ models\ of\ variant\ of\ variant\ models\ of\ variant\ of\ of\ variant\ of\ va$	de
2.	52

List of tables

Table	1.1: Effectiveness	and	application	of	various	cooling	and	lubrication
mechai	nisms[7].							2
Table 2	2.1 : Properties of ni	troger	1.					6
Table 2	2.2 : Nitrogen surfac	e heat	transfer coef	ficie	nt from di	fferent pu	ıblishe	ed papers. 9
Table 2	2.3: Cryogenic coolir	ıg met	thod [26].					10
Table 3	3.1 : Input factors se	lected	for the design	n.				20
Table 3	3.2 : Table of functio	n, con	straint and ob	ject	ive for ma	terial sele	ection.	22
Table 3	3.3 : Material proper	ties.						25
Table 3	3.4 : User-defined m	esh pr	operties.					27
Table 4	l.1 : Findings from A	NOVA	A for Von Mise	s str	ess.			47
Table 4	1.2 : Findings from A	NOVA	\ for maximur	n dei	formation	_		48

Nomenclature

Abbreviations & acronyms

Computer-aided design

CAD

CBN	Cubic boron nitride
CCD	Central composite design
CMQL	Combination of cryogenic CO_2 and oil lubrication
DOE	Design of experiments
FCOF	Function, constraint, objective, and free variables
FEA	Finite element analysis
FEM	Finite element modelling
FOS	Factor of safety
LCO_2	Liquid Carbon dioxide
LN_2	Liquid nitrogen

RSM Response surface method

Performance index

SHTC Surface heat transfer coefficient

Minimum quantity lubrication

TPMS Triply periodic minimal surfaces

Other symbols

MQL

PΙ

- *h* Convective heat transfer coefficient
- H Enthalpy
- K_{IC} Fracture toughness
- ε Normal strain
- σ Normal stress
- ν Poisson's ratio
- *P* Pressure

- γ Shear strain
- au Shear stress
- *T* Temperature
- k Thermal conductivity
- e Volumetric strain
- E Young's modulus

Material Properties

- *μ* Dynamic viscosity
- μ_{JT} Joule-Thomson coefficient
- λ Lamé's constant
- G Shear modulus
- C_p Specific heat capacity at constant pressure
- k Thermal conductivity

Chapter 1

Introduction and background

1.1. Background

Metal cutting or machining is a core material removal process that forms chips and is widely used across the industry to manufacture precise components. When the cutting tool engages a rotating Workpiece with a fixed feed, a chip of material is formed by the tool penetrating the workpiece[1]. In machining technologies such as turning, the process generates significant mechanical and thermal loads due to plastic deformation and friction, resulting in chip formation and heat concentration in the cutting zone[2]. The significant amount of heat is carried by the chips, and a considerable amount of heat remains within the tool, particularly at the cutting edge and tool tip [3]. Excessive heat loads adversely affect tool life, surface integrity, and dimensional accuracy. To mitigate these effects, conventional cooling methods have been widely utilised. The use of water as a coolant dates back to the 16th century as an early cooling fluid [4]. However, the use of plain water led to corrosion and a lack of lubrication. This led to the development of mineral oil-based cutting fluids. Cutting fluids play a major role in machining by reducing abrasion through lubrication, promoting efficient heat removal from the cutting zone, and consequently decreasing thermal and chemical wear on the tool, which leads to improved surface quality of the finished component [5][6], which became common in the early 20th century in the machining of steel alloys. However, these methods have increasingly raised concerns about environmental impact, user health, and disposal costs [7]. As a solution to this problem, MOL was introduced. MOL can contribute to an increase in cutting speed and tool life by providing effective lubrication at the cutting interface. However, the cooling performance is caused by friction reduction, making it less efficient in dissipating a high amount of heat from the cutting area [8]. Consequently, the focus in recent years has shifted towards sustainable and high-performance alternatives such as cryogenic cooling.

Very early cryogenic cooling research was introduced in the middle of the 20th century to overcome the drawbacks of the conventional cooling methods [9][10]. Cryogenic machining techniques provide notable benefits, including the production of contamination-free surfaces and the reduction of white layer formation, both of which enhance the fatigue life of the machined component [11]. The other key advantage of using cryogenic fluids, particularly liquid nitrogen and liquid carbon dioxide, is their high cooling performance due to the huge temperature difference between the fluid and cutting zone, ability to evaporate at atmospheric conditions by absorbing heat from the cutting zone. These fluids do not generate any harmful fumes because of their inert nature [11].

1.2. Comparison of cooling strategies

As indicated in Table 1.1, different cooling methods offer various degrees of effectiveness depending on their application and mechanism of action [7].

Effect of the cooling and lubricant	Flood (emulsion/oil)	Dry (compressed air)	MQL (oil)	Cryogenic (LN₂)	Hybrid (LN ₂ + MQL)
Cooling	Good	Poor	Marginal	Excellent	Excellent
Lubrication	Excellent	Poor	Excellent	Marginal	Excellent
Chip Removal	Good	Good	Marginal	Good	Good
Machine Cooling	Good	Poor	Poor	Marginal	Marginal
Workpiece Cooling	Good	Poor	Poor	Good	Good
Dust/Particle Control	Good	Poor	Marginal	Marginal	Good
Product Quality (Surface Integrity)	Good	Poor	Marginal	Excellent	Excellent

Table 1.1: Effectiveness and application of various cooling and lubrication mechanisms[7].

The studies show Flood cooling with emulsion or oil, for example, offers good cooling ability with excellent lubrication, but it poses environmental concerns. In dry machining, the use of fluid is totally eliminated, but it has poor heat dissipation and lubrication, leading to tool wear and poor surface finish. Minimum quantity lubrication (MQL) provides a more environmentally friendly approach with the minimal amount of

lubricants, but it's less suitable for applications involving high-temperature loads, because of its limited cooling performance. In contrast, cryogenic cooling, particularly with liquid nitrogen (LN_2), stands out by providing excellent cooling without generating any residue on the surface of the workpiece; however, with marginal lubrication efficiency.

1.3. Cryogenic application in machining

Cryogenic technology can be applied in three different ways in the machining process. The first and most common way is the application of cryogenic cooling directly into the cutting zone, in which the cryogenic fluid, typically liquid nitrogen or liquid carbon dioxide, is used. This method is aimed at dissipating the heat at the tool-chip interface during machining and enhances the surface quality and reduces the tool wear rate.

The Second approach is cryo-treatment of cutting tools, also known as cryo-treatment to improve the tool's resistance to wear by modifying the tool's microstructure before use.

The third method is Cryogenic processing of the workpiece material, in which the workpiece is precooled or maintained under cryogenic conditions to improve machinability [11]. These three applications of Cryogenic technology are illustrated in Figure 1.1, which shows the different cryogenic technologies based on their point of application.

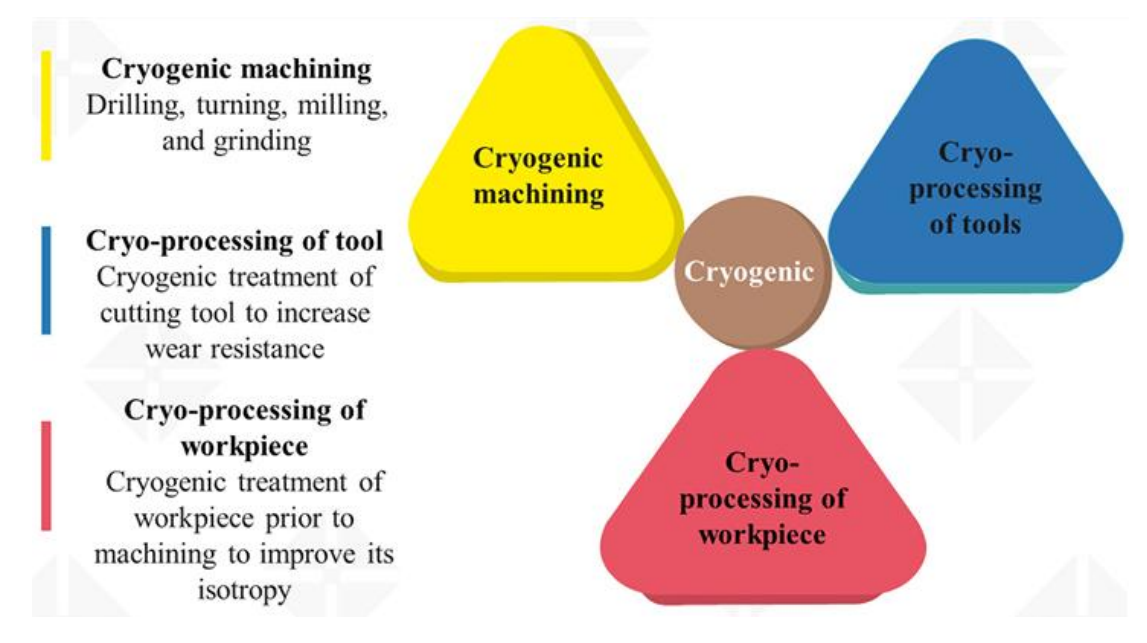


Figure 1.1: Cryogenic machining and processing application [11].

1.4. Thesis structure

This thesis is organized into five chapters, each providing a specific stage of the research process:

Chapter 1: Introduction

Introduces the metal cutting and outlines the significance of temperature control in machining technologies. It highlights the drawbacks of conventional cooling mechanisms and introduces cryogenic cooling as a sustainable alternative.

• Chapter 2: Literature review

Provides a comprehensive review of cooling strategies used in machining, with more focus on cryogenic cooling. It also discusses Properties of cryogenic coolant, surface heat transfer coefficient of LN_2 presented by different researchers, different approaches of cryogenic cooling used by different researchers, and the tool construction for integrated cooling methods. The chapter is concluded with the problem statement and gap specification from the research literature and the objective and scope of the current work.

• Chapter 3: Methodology

The step-by-step procedures and approaches used in this study are described in this chapter. It details the concept generation and CAD design of the tool, simulation planning with the matrix design by DOE, material selection and assignment, boundary conditions for the simulation, and the setup of thermal and structural finite element method (FEM) simulations.

• Chapter 4: Results and discussion

Presents the results from the thermal and structural simulations for temperature distribution and stress results. The results are interpreted and compared with the trends from the literature review and the mechanical properties of the materials to ensure the structural stability of the designed tool.

• Chapter 5: Conclusion

This chapter summarizes the findings and outcomes from the research, assesses the feasibility of the proposed integrated chamber design for the internal cryogenic cooling concept, and discusses the limitations faced. The chapter also recommends future work.

Chapter 2

Literature review

Cryogenic cooling has emerged as a sustainable alternative in machining operations, particularly for hard-to-machine materials like titanium alloys, nickel-based super alloys, and hardened steels to conventional cutting fluids. Traditional lubrication and cooling methods, such as flood cooling and minimum quantity lubrication (MQL), pose significant environmental and health concerns due to fluid waste and mist formation [12].

Bagherzadeh & Budak [13] introduced a new approach called CMQL (combination of cryogenic CO_2 and oil lubrication), by investigating the effectiveness of combining the cryogenic cooling concept with minimum quantity lubrication (MQL). Their research showed a significant improvement in tool life, extending by up to 345% for Ti6Al4V, and reduced cutting forces compared to conventional cooling methods. Furthermore, their approach enhanced surface finish, reduced temperature at the cutting zone, and minimized tool wear through improved cooling.

According to the study by Yap [14]. The application of LN_2 as a cooling method has different advantages, including reducing thermal damage to the tool and workpiece, improving surface finish quality, and minimizing tool wear. The study also highlights that the thermal properties of LN_2 , such as high heat capacity and low boiling point make it an effective coolant for high-temperature machining processes. The review paper also presented different roles of cryogenic cooling in machining different materials, superalloys (titanium alloys, Inconel alloy, tantalum alloy, etc.), ferrous metals, viscoelastic polymers and elastomers. As a result, they presented that the role of cryogen is slightly different in machining different materials.

Cryogenic cooling, particularly using liquid nitrogen (LN_2), offers several advantages such as reduced tool wear, improved surface finish, and lower thermal damage to the workpiece [12][15].

Courbon et al [16] presented in their study the influence on the tribological properties of Ti6Al4V and Inconel 718 alloys while using cryogenic lubrication. The study used an open tribological setup to simulate the contact conditions during machining, particularly focusing on the examination of heat transfer, friction coefficient and adhesion at the

interface between the cutting tool and the work material. The paper concluded that the heat generated during machining can effectively be reduced by cryogenic lubrication, especially with liquid nitrogen, but its effect on friction varies depending on the work material.

The paper by Pusavec F [17] investigates the effects of cryogenic cooling on machining porous tungsten, a challenging material to machine due to its thermal and wear characteristics. In the study, the author focused on liquid nitrogen cooling and explored the optimization of the parameters to obtain the specified machining surface quality of the final product. The result of the study shows cryogenic machining is capable of producing unsmeared surfaces that satisfies the industry standards which has never been achieved for any other cooling methods.

2.1. Cryogenic properties

Due to its unique thermophysical properties, cryogenic cooling, particularly liquid nitrogen, has gained significant attention in the field of machining. LN_2 has a boiling point of -196 °C at standard atmospheric pressure, and it is widely used due to its exceptional ability to reduce cutting temperatures and enhance tool life by minimising thermal damage to the tool material. Pusavec et al [18] in their paper, they mentioned that LN_2 ensures efficient heat transfer from the cutting zone, allowing better temperature control during the machining of hard-to-cut materials such as Inconel and titanium alloys due to their high thermal conductivity and low viscosity.

The property of liquid and gas nitrogen is summarised in the Table 2.1 below, as referred to [18].

	Density(Kg/m³)	Cp(KJ/KgK)	μ(Pas)	k (W/mK)
N ₂ liquid	803.6	2.046	1.463 × 10 ⁻⁴	1.320×10 ⁻¹
N ₂ gas	4.979	1.351	0.05331×10 ⁻⁴	0.07658× 10 ⁻¹

Table 2.1: Properties of nitrogen.

In another study, B. Dilip Jerold and M. Pradeep Kumar did an experimental comparison between carbon dioxide and liquid nitrogen cryogenic coolants in turning of AISI 1045 steel, and they found that the application of LN_2 reduced the cutting temperature to the maximum when compared to wet or CO_2 machining. This is due to the low boiling point

(-196°C) of LN_2 [19]. In their research they also investigated that Application of CO_2 and LN_2 reduced the cutting temperature by about 6–21% and 9–34% when compared to wet machining respectively. Cryogenic LN_2 provided the maximum benefit of reduction in the cutting temperature, and it reduced about 3–17% of cutting temperature when compared to CO_2 application.

In comparison to LN₂, while also used in cryogenic machining, it has a higher boiling point, which limits its cooling capability compared to LN₂. CO₂ undergoes Joule–Thomson expansion in which it transforms into a gas-snow mixture when rapidly expanded, which, although effective in certain applications, does not offer the same level of cooling efficiency or localised heat management as LN₂ [19]. The mathematical representation of this effect is given by the Joule–Thomson coefficient:

$$\mu_{\rm JT} = \left(\frac{\partial T}{\partial P}\right)_H \tag{2.1}$$

where μ_{JT} is the Joule–Thomson coefficient, T is the temperature, P is the pressure, and the subscript H denotes constant enthalpy [20].

However, CO_2 has been found to be effective in combination with other lubrication methods, such as minimum quantity lubrication (MQL), providing a more eco-friendly solution in some cases [21].

2.2. Surface heat transfer coefficients in cryogenic cooling

As the main objective of the cryogenic fluid is to dissipate the heat generated during the cutting operation, the quantification of the heat transfer between the cryogenic fluid with the cutting tool, and the machined surface remains an issue to be addressed [7].

The paper by Pusavec et al., 2016b [22] presents the effect of nitrogen phase on heat transfer coefficient during cryogenic machining. The authors made a comparison of the cooling performance of liquid nitrogen and nitrogen gas in terms of heat transfer efficiency. The result from the paper showed heat transfer efficiency of liquid nitrogen is significantly higher than that of nitrogen gas. For the liquid nitrogen, the heat transfer ranged from 23270 W/(m².K) to 74950 W/(m².K), depending on the overheat temperature, whereas it is lower for nitrogen gas. As a result of higher heat transfer, liquid nitrogen gains higher thermal conductivity and specific heat, which allows it to absorb more heat from the cutting zone. From the study, it is concluded that better

cooling efficiency is offered by liquid nitrogen, and it should be the preferred choice in cryogenic machining for improved performance and longer tool life.

In Cryogenic machining, cooling efficiency is highly affected by the surface heat transfer coefficient, especially when using liquified nitrogen as a coolant. A study by Hribersek et al [23] focused on determining the heat transfer coefficient between liquefied nitrogen and Inconel 718 during Cryogenic machining. The results from the study revealed that the heat transfer coefficient is highly temperature dependent, peaking at around 75,000 W/($m^2 \cdot K$) when nitrogen was in its liquid phase at -196°C. The authors also investigated that as nitrogen transitions to a gaseous phase, a significant drop in the heat transfer coefficient to approximately 15000 W/($m^2 \cdot K$) appears.

Y. Wang et al [24] in their paper investigated the effect of LN_2 mass flow rate, jet distance, and nitrogen phase based on a self-developed experimental platform to achieve different cooling performance using SHTC as an evaluation indicator. The authors concluded that the overall SHTC and peak SHTC value increase significantly as the LN_2 mass flow rate increases and the jet distance decreases. But the SHTC is more sensitive to jet distance in comparison to flow rate at the initial stage. Then, the SHTC of gaseous phase nitrogen is only $15000W/(m^2.K)$. It is much lower than that of LN_2 . So, supplying an abundant amount of liquid nitrogen during cryogenic machining is critical.

Another paper investigates the critical role of the nitrogen phase (liquid vs. gas) in determining the surface heat transfer coefficient (HTC) during cryogenic machining, specifically when using liquid nitrogen (LN_2) for cooling. The authors developed a method to monitor and control the nitrogen phase at the delivery nozzle by an optical sensor, which is crucial for stable machining performance. They established experimental surface heat transfer coefficients as a function of the overheat temperature ($T_{overheat}$) and observed that the HTC is highly dependent on the nitrogen phase and temperature differences between the cutting surface and the cooling fluid. The study found that superior cooling is achieved using liquid nitrogen compared to its gaseous counterpart, as it induces higher heat flux due to boiling heat transfer. These findings emphasize the importance of nitrogen phase control in optimizing cooling efficiency and machining performance, with significant implications for tool life and material integrity in cryogenic machining processes [18].

Different authors investigated a different range of heat transfer coefficients of LN_2 based on different factors under varying operational and experimental conditions. A

comprehensive summary of the heat transfer coefficient values reported in the literature is presented in Table 2.2 below.

	LN ₂ HTC (W/m ² .K)	Authors
1.	48270 - 74950	S. Y. Hong and Y. Ding [25]
2.	23300 - 46800	M. Dix [26]
3.	20000 (constant)	G. Rotella [27], M. F. Novella [28]
4.	20000 (constant)	A. H. Kheireddine [29]
5.	2327- 74950	F. Pusavec [18]
6.	15000 - 75000	M. Hribersek [23]

Table 2.2: Nitrogen surface heat transfer coefficient from different published papers.

2.3. Cooling approaches using cryogenic coolants

Ding et al [30] Explore applications of cryogenic cooling in the machining process, particularly in turning operations. The authors focused on modelling and simulation of cryogenic cooling using liquid nitrogen to improve efficiency for tool temperature management. Their method involved both experimental and simulation approaches. They evaluated the effect of cryogenic cooling on tool wear and surface quality during machining by conducting experiments and they also employed FEM simulation to predict the thermal behaviour of the cutting tool under different cooling conditions. The result showed the reduction of tool wear and improvement of surface finish due to significant reduction of cutting temperature by cryogenic cooling. The authors also investigated influence by the positioning of the cooling channel and tool geometry concluding that they are critical factors for optimizing the cooling effectiveness.

In another paper by Umbrello et al [31] the authors investigated the effect on surface integrity in the hard machining of AISI52100 steel, comparing it with dry machining. The authors conducted a series of dry machining and cryogenic cooling experiments using Cubic boron nitride (CBN) tools under different conditions. The cryogenic cooling system utilized is liquified nitrogen (-196°C) in their experiment. The result of their experiment showed significant of white layer thickness while using cryogenic cooling when compared to dry machining and provided superior surface roughness. The study concluded that product life and machining performance, particularly in terms of surface quality and fatigue resistance, are enhanced using cryogenic machining techniques.

The study by Biermann & Hartmann [32] investigates the potential of cryogenic cooling using CO_2 snow jets to reduce burr formation during drilling operations. Burrs, undesired material projections, not only affect component quality and functionality but also contribute significantly to production costs, especially when deburring is required. The authors proposed a burr minimization approach that cools the exit side of the workpiece using CO_2 jets.

In a comprehensive review paper by Yildiz & Nalbant [12] several cryogenic cooling strategies, highlighting the advantage of using liquid nitrogen (LN₂) to manage heat generation during cutting operations were reviewed. Their study examined methods such as indirect cooling, focused jet cooling, and workpiece precooling, as shown Table 2.3 below. The authors investigated that compared to dry and conventionally cooled machining, cryogenic system offered enhanced dimensional accuracy and environmental benefits. However, they emphasized that the success of cryogenic machining is highly dependent on variables such as material properties, tool geometry, and cutting conditions.

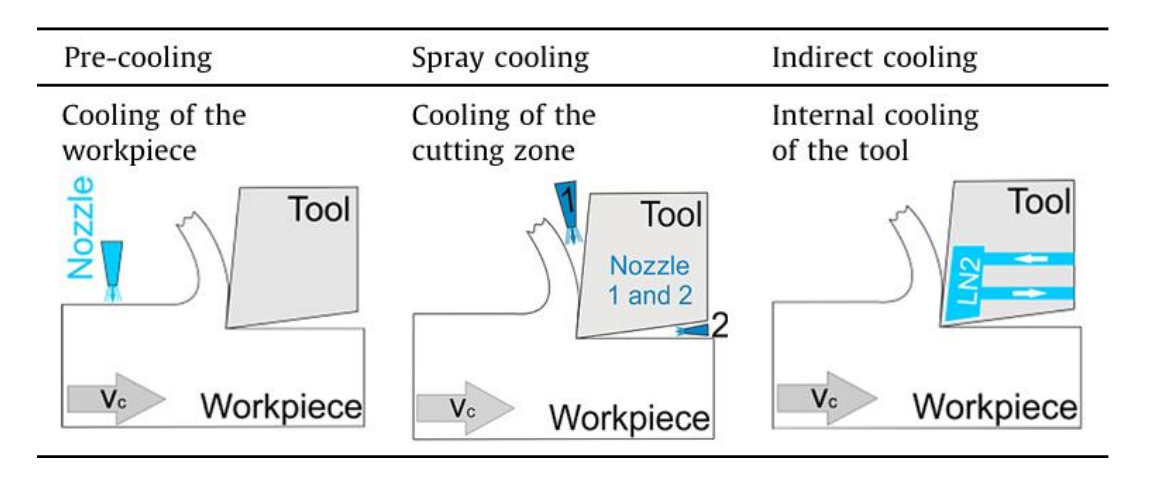


Table 2.3: Cryogenic cooling method [26].

The study by Dix et al [26] present a detailed investigation into the efficiency and modelling of cryogenic cooling during drilling process. Simulations by the author revealed that while extremely high temperatures still occurred at the chip-tool interface (up to 820°C), cryogenic cooling drastically reduced tool temperature by up to 50% compared to dry drilling.

Additionally, Bermingham et al [33] studied the impact of cryogenic cooling on tool life and cutting forces in machining hard materials. Their study demonstrated that cryogenic cooling with LN_2 could reduce cutting forces and enhance surface quality, leading to

prolonged tool life. They noted, however, that cryogenic cooling effectiveness was more noticeable at lower cutting speeds.

In their study, Chaabani et al [34] make a comparison on the performance of liquid nitrogen (LN_2) and liquid carbon dioxide (LCO_2) as cryogenic coolants during finishing turning of Inconel 718. In their research, they investigated that LCO_2 cooling led to better tool life, lower surface roughness, and more beneficial compressive residual stresses than LN_2 . They also highlighted LCO_2 as a more effective cryogenic coolant for enhancing machining quality and tool performance in their research.

Another paper Dhananchezian et al [35] studied the effect of cryogenic cooling On Machinability Characteristics During Turning Duplex Stainless Steel 2205, in their study the authors investigated that using liquid nitrogen as a coolant results in a significant reduction of cutting temperature and forces. The liquid nitrogen as coolant reduced the cutting temperature within the cutting conditions by 53 - 58 % over dry turning and that the main cutting force and feed force was decreased by about 30 - 41 % and 33 – 43 % with application of liquid nitrogen under cryogenic cooling when compared to dry turning. The paper also investigated improvement in roughness values and better results in terms of machinability indices when compared to dry cutting environments.

2.4. Tool construction

The integration of the liquid nitrogen (LN_2) delivery system into the tool structure is a key engineering challenge in the development of cryogenic cooling systems for machining. Z. Y. Wang et al [36] constructed a specialized tool holder that incorporated copper tubing routed internally to deliver LN_2 directly to the cutting edge. The tool holder was modified to include a sealed chamber around the tool insert, allowing LN_2 to flow through internal passages and exit precisely at the tool-chip interface as indicated in Figure 2.1 below. To minimize thermal losses and prevent condensation on external surfaces, insulation materials were applied around the coolant channels. Similarly, Z. Y. Wang et al [37] designed a cryogenic tool setup with LN_2 delivered through a miniature nozzle integrated into the tool body, where fine-gauge thermocouples were embedded near the cutting edge to monitor temperature, in this construction they introduced direct cooling of the cutting zone while maintaining tool rigidity and structural integrity. They included minimizing flow path distance to reduce cooling delay, sealing joints to prevent LN_2 leakage, and maintaining a compact, balanced geometry suitable for high-speed operations as a Critical design consideration. The internal cooling concept thus demands

precise machining of internal channels, robust material selection for thermal and mechanical stresses, and careful integration to ensure uninterrupted coolant delivery during cutting.

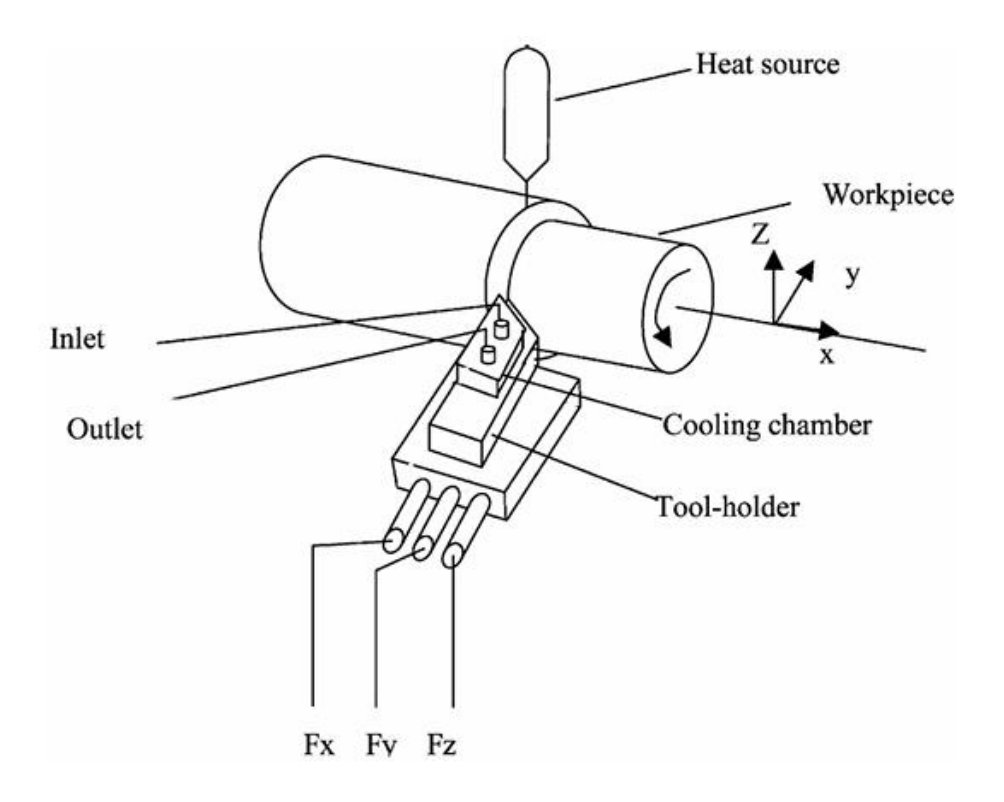


Figure 2.1: Illustration of hybrid machining used by Z.Y. Wang [36].

Novella et al [28] redesigned and investigated the thermo-mechanical behaviour of a tool holder aimed at reducing geometrical deviations during cryogenic machining of Ti6Al4V alloy. in their study, they combined experimental tests using liquid nitrogen (LN_2) cooling with a FEM for thermomechanical analysis. They incorporated an embedded cartridge heater into the tool holder to compensate for thermal contraction caused by the LN_2 cooling. Results showed that the redesigned tool holder significantly reduced dimensional deviations by approximately 38% at 150 W heater power compared to the original design. In their study, temperature distribution and thermal deformation were accurately predicted by the validated numerical model, highlighting the importance of thermal management in improving machining accuracy under cryogenic conditions.

The study on the design and performance of an internal cooling turning tool with a microchannel by Peng et al [38] investigates the effectiveness of internal cooling in machining applications. The research highlights how microchannel-based cooling enhances heat dissipation, reduces thermal damage, and improves tool life compared to

conventional external cooling methods. In their design, they created an interior cavity in the tool, with the coolant inlet located at the end of the cavity. Two microchannels, of the same diameter, are designed to direct fluid towards the major and minor flank faces. Figure 2.2 shows the construction geometry for the internal microchannel cooled turning tool by Peng et al [38].

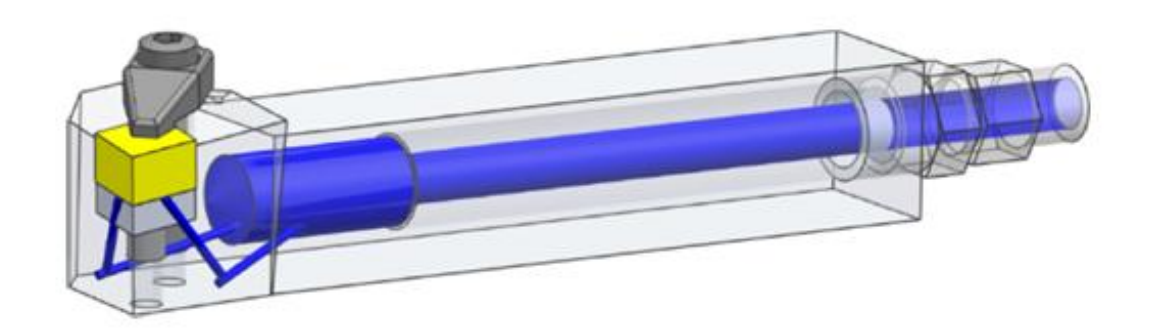


Figure 2.2: Internal micro-channel cooled tool [38].

In their paper, Minton et al [39] replaced the usual shim found on conventional tooling with a cooling block, into which microchannels are machined into a small cavity situated just below the cutting tip. The authors used the jet impregnation method, by which the coolant is directed through the cooling block and sprayed onto the underside of the cutting insert. This cooling system aims to effectively manage the high temperatures generated during machining, which can lead to thermal wear and reduced tool life, by delivering coolant as close to the cutting zone as possible. By integrating this system, the authors significantly improved heat dissipation, reducing the temperature at the cutting tip and minimizing wear mechanisms typically associated with excessive heat. The design highlights the effectiveness of embedding cooling technology within the tool holder, resulting in extended tool life and enhanced surface finish quality.

Another study by Chiou et al [40] investigates a different approach for tool construction in which the performance of a cutting tool embedded with a heat pipe for reducing cutting temperature and wear in machining processes. The authors utilized Finite Element Analysis (FEA) to model the temperature distribution during machining, specifically focusing on the tool-chip interface. The authors also conducted an experiment where a cutting tool was embedded with a heat pipe. Their result demonstrates a significant reduction in cutting tool temperature, leading to a decrease in tool wear and prolonged tool life. Furthermore, the study highlighted the minimization of the environmental impact of cutting fluids, offering an alternative to traditional cooling methods using embedded heat pipes in cutting tools.

In the paper by Uhlmann et al [41] The authors present the development of an additively manufactured tool holder with an internal cooling designed for turning operations. In their design, to enhance the cooling efficiency, based on the expansion of liquid CO_2 , they incorporated Triply periodic minimal surfaces (TPMS) lattice structures. Both simulation and experimental methods were involved in the study to validate the design and functionality. The heat transfer properties of the TPMS structures are assessed using ANSYS software and the tool holder was fabricated using laser powder bed fusion with 316L Stainless Steel in this paper. The result from the simulation and experimental tests of this paper showed a significant reduction of the cutting-edge temperature compared to an uncooled tool holder and emphasizes the potential of additive manufacturing for creating customized, efficient cooling systems for machining tools, contributing to higher productivity and improved sustainability in industrial applications.

2.5. Task specification

2.5.1. Problem statement

As indicated in the literature review, studies highlighted the advantage of using cryogenic cooling in machining processes, but the integration of the liquid nitrogen (LN_2) delivery system into the tool structure is a key engineering challenge[42][43][44]. This difficulty comes from the need for precise delivery of the coolant and thermal insulation. Another critical limitation is the reduction of the heat transfer coefficient when LN_2 encounters the hot solid surface. This phenomenon is attributed to the Leidenfrost effect, where the vapour layer forms between the cryogenic liquid and the heated surface, insulating the tool or workpiece and significantly reducing the heat transfer effectiveness [23]. The current research work aims to integrate the cooling chamber directly into the turning tool head, positioned below the cutting insert support, to address the gaps in the previous research works.

2.6. Objective of the study

This thesis work will focus on a new approach to designing a turning tool with an integrated cooling chamber beneath the cutting insert support, which can be used for the application of LN_2 as a cooling material. The study will focus on conducting comprehensive thermal analysis and structural analysis using ANSYS Simulation software. The primary aim is to evaluate the feasibility and structural integrity of the designed tool; The research aims to determine whether the tool holder can withstand thermal and mechanical loads that arise during cryogenic turning operations.

2.6.1. Specific objectives

The following are the main objectives of this research

- 1. To design the 3D model of the turning tool.
 - Design the turning tool head with an integrated expansion chamber for LN₂: the chamber will be strategically placed beneath the cutting insert support to allow efficient cooling during machining
- 2. To conduct steady-state thermal and static structural analysis
 - Steady state thermal analysis to evaluate the distribution of temperature under the cryogenic machining using ANSYS 2024 R2.
 - Static structural analysis will be performed to assess the strength and deformation of the tool during operation under cryogenic machining and prove the strength of the material to be designed.
 - Simulation will help to validate the stability, thermal behaviour, and tool strength during machining
- 3. To carry out a parametric study to assess the influence of the key factors
 - Investigate the effect of different parameters such as Heat transfer coefficient (HTC), tool tip temperature, atmospheric temperature, expansion chamber size, and insulation method
 - Use the response surface method (RSM) to investigate the effect of different combinations of the parameters

2.7. Scope of the study

This research work investigates the integration of a cooling mechanism within the turning tool by designing the internal liquid nitrogen cooling chamber on the tool head. The scope of the study is the design and modelling of the tool geometry with the development of insulation strategies, assessment of thermal and structural stability using FEA, and a parametric study using the response surface method (RSM).

This research work relies entirely on simulation techniques, using steady-state thermal and static structural analysis.

The experimental testing, dynamic thermal analysis, and wear modelling are not included in this work. The outcomes aim to provide design insights for the future development of internally cooled cutting tools suitable for cryogenic machining.

Chapter 3

Methodology

This chapter outlines the methodological approach employed to develop and evaluate a novel internal cryogenic cooling concept for a turning tool using liquid nitrogen (LN_2). The process consists of concept generation with focus on integrating LN_2 cooling within the tool structure, digital tool modelling, thermal and structural analysis using FEM, which enables the cost effective and detailed evaluation of the tools behaviour under machining load and cryogenic cooling. This approach allows virtual testing of the designed tool model. To systematically investigate the effects of key parameters design of experiment (DOE) is utilized to determine the simulation matrix. After the simulation, response surface method (RSM) is applied to investigate the effects of different combinations of the parameters.

3.1. Concept generation and tool modelling

Two primary concepts were initially developed, each utilising different insulation methods to analyse the influence of insulation strategies on the performance of an internally cooled turning tool.

- Model 1: model with an insulation coating applied to the internal surface of the expansion chamber
- Model 2: incorporates an insulation pad positioned between the tool head and the shank

Each concept was further divided into different variants by modifying the size of the expansion chamber, one chamber with a larger size and another chamber with a smaller size, which in total gives four different design models. The key design in all four variants is the integration of the LN_2 expansion chamber directly beneath the cutting insert support within the tool head. The chamber is designed in such a way that it remains close to the heat generation zone during machining and provides an exit for the evaporated nitrogen. This ensures that the cryogen can absorb and dissipate heat from the cutting insert more effectively. The tool geometry is specifically designed to house the expansion chamber without compromising the mechanical strength or rigidity of the cutting tool during the cutting operations.

All parts were designed and developed using AUTODESK INVENTOR 2025, with the tool system designed in a modular part to allow flexible configurations and analysis. The overall tool size for all four designs was maintained within the dimensional range of a standard turning tool [45].

The following parts were designed and then assembled

- 1. Tool head
- 2. Cutting insert
- 3. Cutting insert support
- 4. Tool shank
- 5. Insulation coating (for model 1 only)
- 6. Insulation pad (for model 2 only)

The tool is assembled based on the modular architecture, in which the tool head will be separately designed and additively manufactured. This separately manufactured tool head is then assembled to the standard tool shank by using a mechanical bolt on interface. This connection mechanism allows secure attachment, ease of maintenance, and replacement flexibility, and model suitability to be additively manufactured.

On another way cutting insert is first brazed to the insert support. Active brazing alloys containing elements like titanium (Ti) are commonly used to ensure strong interfacial bonding with the chemically inert CBN surface [46]. After brazing, to connect the cutting insert and insert support assembly to the tool head, a wedge clamp mechanism will be utilised. This system ensures accurate positioning and high clamping force, suitable for withstanding the mechanical and thermal stresses involved in cryogenic machining.

Figure 3.1 below shows the tool head design and full assembly configuration for both models.

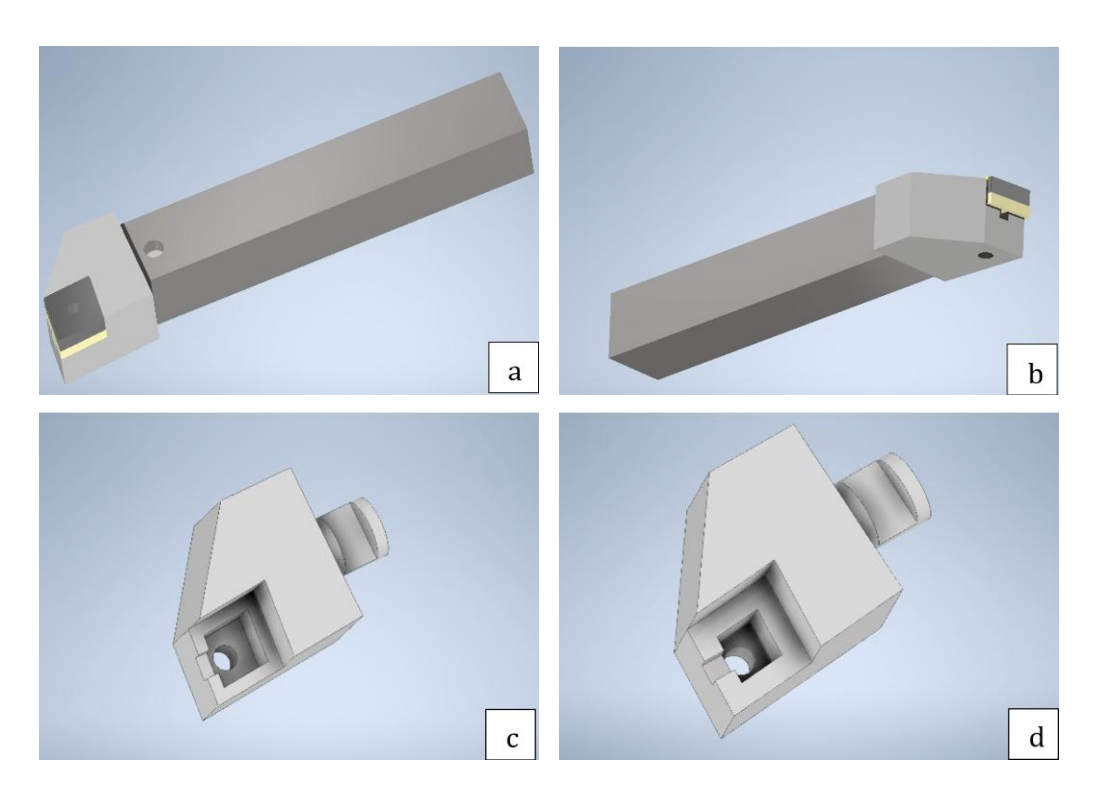


Figure 3.1: a) Turning tool assembly with integrated insulation pad, b) with expansion chamber coating, c) tool head with larger expansion chamber, d) tool head with small expansion chamber.

3.2. Simulation planning

Design of experiment approach is employed in this project to study the effect of different variables on the tool. RSM is an efficient statistical technique that is widely used for optimizing processes where multiple factors and their interaction affect the outcome [47]

The factors that mostly affect the cryogenic efficiency of the machining process include LN_2 flow rate, LN_2 phase change, which are highly affecting the HTC value [18], tool tip temperature, Atmospheric temperature, material property, LN_2 chamber size, tool tip temperature, and feed forces. Central composite design (CCD) was selected due to its capability for efficient modelling of second-order responses with a reduced number of runs while still enabling the estimation of curvature effects and interaction terms [47].

The central composite design utilised in this project uses a full factorial core including:

- Three continuous factors: cutting tip temperature, atmospheric temperature, and LN₂ heat transfer coefficient
- Two categorial factors: insulation method and LN₂ expansion chamber

Levels for LN₂ HTC are selected based on relevant ranges found in previously published literature. similarly, the tool tip temperature range is determined based on the literature [48][49][50], ensuring physically realistic simulation scenarios. Categorical factors are derived from design preferences and configurations developed during the concept generation and modelling phase.

The following Table 3.1 shows the input factors used in this project with their respective levels.

Factors	Factor type	Level	Unit
LN ₂ HTC		20,000 – 60,000	W/(m ² .K)
Atmospheric		15 – 30	°C
Temperature	Continuous		
Tool tip		150 – 700	°C
temperature			
Chamber size		small(163.308mm ³)/big(378.246mm ³)	
Insulation method	categorical	chamber coating/insulation pad	

Table 3.1 : Input factors selected for the design.

DOE helps to determine the boundary conditions for each of the simulation arrangements by varying the input parameters.

CCD is particularly effective in modelling complex engineering systems where both linear and quadratic behaviours are expected [51].

Minitab® software was employed to create the DOE. Since CCD develops a design for continuous factors, Minitab® handled categorical variables by creating a separate CCD for each combination of the categorical levels. As a result, a total of 80 simulation orders were generated, including all the possible combinations of the factors across the continuous and categorical factors. These simulation orders are then to be used to guide the FEM simulations for evaluating thermal and structural performance of the tool models. The full simulation matrix, including detailed factor combinations for each run, is provided in Appendix A.

3.3. Simulation study

Following the completion of DOE, a series of Finite Element Method (FEM) simulations are run to systematically evaluate the thermal and mechanical performance of internally cooled tool design under cryogenic conditions. Each of the 80 simulations, which are generated using CCD through Minitab®, is analysed in accordance with the factor combinations. The simulations are run using ANSYS Workbench 2024 R2. Each simulation case corresponds to a specific combination of the design factors such as LN2 chamber size, cutting temperature, atmospheric temperature, LN2 HTC and insulation method as defined by the DOE matrix. For each case of the simulation, the steady state thermal distribution resulting from cryogenic cooling, the Von Mises stress to identify the maximum stress, and the total deformation to assess the tool stability under thermal and mechanical applications will be evaluated. The simulation study collectively provides insights into how different combinations of parameters will affect the performance of the cryogenically cooled turning tool. The simulation setup, material assignment, boundary conditions, meshing strategy, and methods used for both thermal and structural analysis are discussed in the following subsections

3.3.1. Material selection and assignment

Material selection for all the components of the cryogenic turning tool is performed based on the distinct mechanical and thermal requirements for each part during the operation process. Key considerations included during the material selections include thermal shock resistance, structural integrity under high loads, compatibility with liquid nitrogen and manufacturability, particularly additive manufacturing for the tool head materials. Commercial availability is also considered during the material selection and assignment for the simulation.

The tool head is a critical component in the cryogenic turning tool system, serving both as a mechanical support for the cutting insert and as a housing for the internal liquid nitrogen (LN_2) cooling chamber. It must endure the stresses generated during turning and structurally and thermally stable under extreme temperature gradient ranging from cryogenic (-196°C) to elevated temperature during machining. Therefore, appropriate material selection is very essential to ensure functional stability and reliability of the tool.

To systematically select the material, the Granta EduPack software is used. The FCOF methodology (Function, Constraints, Objective, and Free variables) is adopted to define the selection criteria, as outlined in Table 3.2 below.

Function	Ensure the proper support of the cutting insert and housing liquid nitrogen during machining
Objective	Maximize stiffness Maximize strength Maximize toughness Maximize thermal stability
Constraints	Must withstand cryogenic cooling (minimum service temperature ≤ -70°C) High yield/tensile strength (≥1000MPa) Adequate fracture toughness (≥ 20 MPa·√m) Must withstand thermal stresses (maximum service temperature ≥ 500°C)

Table 3.2: Table of function, constraint and objective for material selection.

In addition to the above constraints mentioned in Table 3.2 A low thermal expansion coefficient to reduce the deformation under thermal cycling and good hardness to maintain cutting edge integrity and support the insert are other parameters to select the appropriate material.

After applying all the above constraints using Ansys Granta software, 21 materials remained potential candidates for the selection. These materials include various high-performance tool steels, tungsten carbide composites, and some high-temperature nickel-based superalloys.

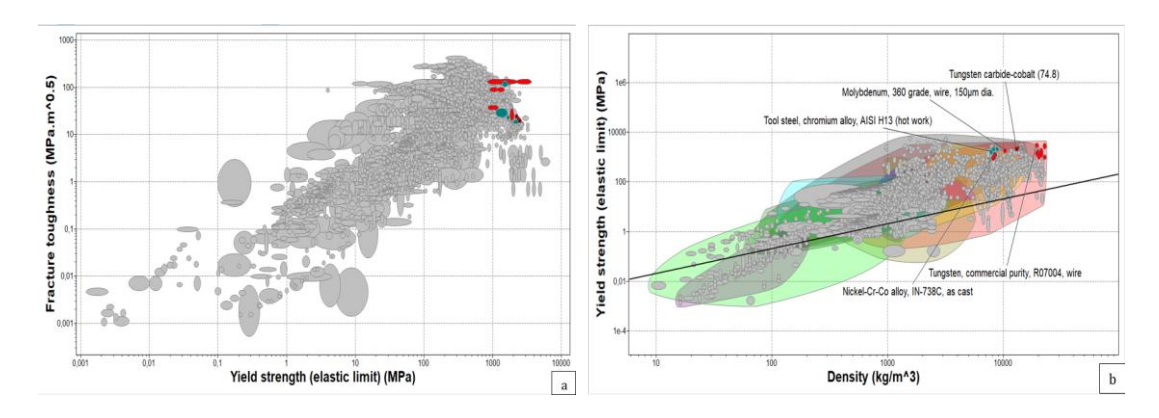


Figure 3.2 : Top 21 candidate materials a) fracture toughness-yield strength graph b) yield strength-density graph.

To further narrow the selection of the material, the performance-based ranking uses a custom performance index derived from the key material constraints for the tool design [52] [53].

$$PI = \frac{K_{ic} * \sigma_{y}}{\alpha * \rho} \tag{3.1}$$

This index prioritizes materials with high toughness and strength, low expansion, and moderate density ideal traits for thermally stable, strong tool heads in dynamic environments.

After applying thermal, mechanical and functional constraints to Granta EduPack software, 9 materials are shortlisted as a suitable candidate for tool head as indicated in Figure 3.3.

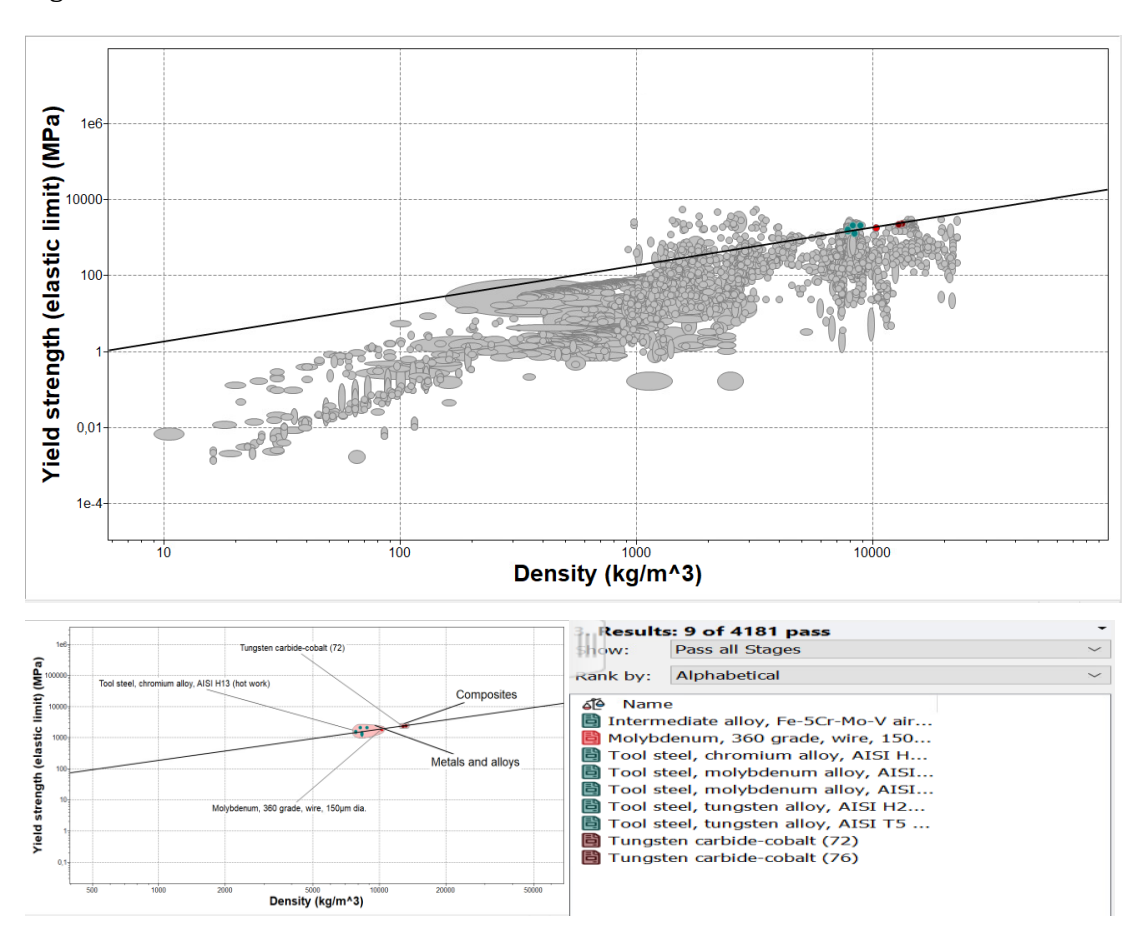


Figure 3.3 : Top 9 candidate materials for the tool head after performance index application.

Among the candidate materials, AISI H13 tool steel is selected based on its superior performance in strength, fracture toughness, thermal stability, and additive manufacturing compatibility. Recent work by Fonseca et al. [54] provides robust

experimental evidence supporting this choice. Their study demonstrated that H13 processed via PBF-LB and tempered at high temperatures can achieve fracture toughness values of up to 87 MPa· m^{1/2} and yield strengths exceeding 1100 MPa. The same material, tool steel AISI H13, is also selected for the tool shank, which is commercially widely applicable for this purpose.

For cutting insert, cubic boron nitride (CBN) is selected due to its exceptional mechanical properties, thermal stability, and commercial availability in hard turning operations. CBN is the second hardest known material after diamond, with the Vickers hardness ranging from 30 to 43 GPa [55]. Its inertness with ferrous materials minimizes tool wear due to chemical reactions, making it particularly suitable for machining hardened steels and superalloys [56]. It is also suitable for efficient heat dissipation from the cutting zone, facilitated by its high thermal conductivity [57].

Cemented carbide (WC-Co) is selected for the insert support due to its high hardness and toughness, which makes it suitable for supporting cutting inserts under high-stress conditions. These properties of WC-Co are influenced by the cobalt content and tungsten carbide grain size, with finer grain size and optimal cobalt content optimizing the properties [58]. Cemented carbide is also widely used commercially to manufacture cutting inserts and their supports.

In this project, two different insulation methods will be considered to enhance the thermal management within the cutting tool

Silicon-based aerogel is selected for the coating of the LN_2 expansion chamber due to its exceptional thermal insulation properties, low density, and adaptability for high-temperature applications. It exhibits very low thermal conductivity as low as 0.014 $W \cdot m^{-1} \cdot K^{-1}$; this makes it highly effective for thermal insulation [59].

On the other hand, for the insulation pad to be placed between the tool head and the tool shank, alumina (Al_2O_3) is selected as the optimal material due to its exceptional thermal insulation properties, mechanical strength, and chemical stability. Alumina exhibits a low thermal conductivity of approximately 25–30 W/(m·K) at room temperature [60].

The important properties of the materials for the simulation are summarized in Table 3.3 for all the materials

Material	Density	Thermal	Yield	Young's	Poisons
	(Kg/m ³)	conductivity	strength(MPa)	modulus	ratio
		(W/(m°C))		(GPa)	
CBN	3840	150		500	0.15
WC-Co	14500	100	750	550	0.22
Tool steel H13	7765	25	1200	220	0.29
Alumina	3800	24.7		300	0.22
Silicon-based Aerogel	150	0.015		0.05	0.2

Table 3.3: Material properties.

3.3.2. Meshing strategy

User-defined meshing strategy is used with different meshing sizes for different parts to optimize accuracy and computational efficiency of the finite element analysis (FEA) model.

Mesh consists of varying element sizes assigned to different parts of the model based on their functional importance and expected variations of the solution value. Finer mesh density characterized by a smaller mesh element size is applied in regions where high gradients of temperature, stress, or displacement are anticipated, such as the tool cutting insert, the LN_2 expansion chamber, and the cutting support. Larger mesh elements are applied in areas with relatively uniform fields. This type of meshing strategy enhances the reliability of the simulation result and significantly improves the overall feasibility and efficiency of the FEA model. The total number of elements in the model varies for each model

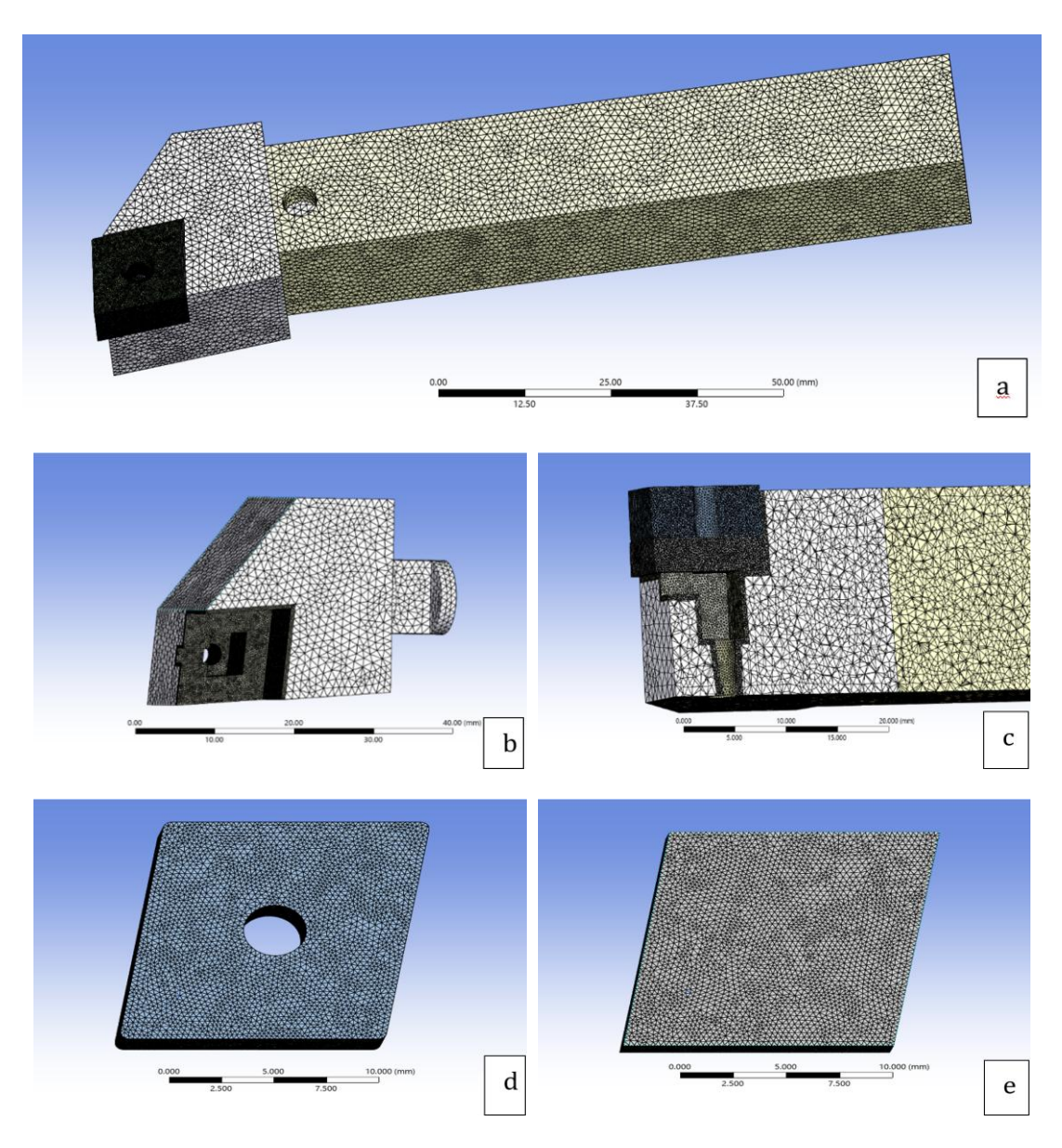


Figure 3.4 : Meshing strategies for variant 1 with chamber coating a) assembled part b) tool head with internal chamber coating c) sectioned part of the assembly d) cutting insert e) insert support.

The meshing strategy employed a hybrid element method with predominantly quadratic tetrahedral elements (Tet10) and a smaller number of quadratic hexahedral elements (Hex20) for geometric complexity and simulation accuracy. A fine mech element size of 250 micrometers was applied to the insulation coating, cutting insert, and insert support where high thermal and mechanical loads are expected. For the tool head and tool shank, a coarser mesh with 1000 micrometers is used, as these regions experience relatively uniform temperature distribution and stress. The meshing strategy enabled precise modelling of the internal cooling chamber with the quadratic order of elements combined with tetrahedral flexibility.

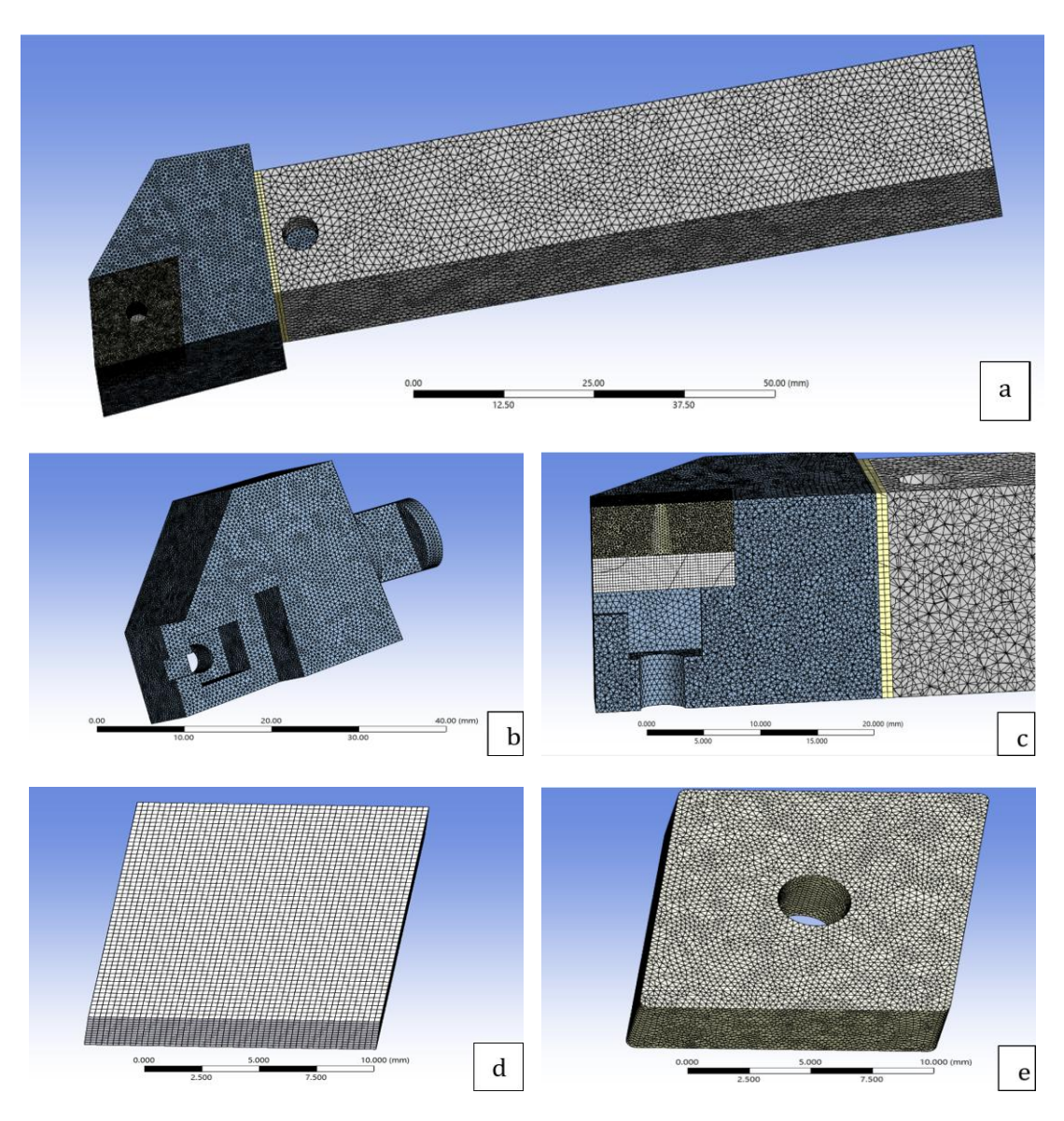


Figure 3.5: meshing strategies of variant 2 with insulation pad between head and shank a) tool assembly b) tool head c) sectioned part of the assembly d)insert support e) cutting insert.

The meshing strategies for variant 2 can be summarized in the following Table 3.4.

Parts	Mesh size (μm)	Element order
Tool shank	1000	Quadratic
Tool head	500	Quadratic
Cutting insert	250	Quadratic
Insert support	250	Quadratic
Insulation pad	500	Quadratic

Table 3.4: User-defined mesh properties.

3.3.3. Boundary conditions

The boundary conditions are defined to analyse the thermal and structural properties of

the tool under cryogenic machining conditions. The conditions govern the proper

interaction of the tool model with its environment and applied loads to ensure that the

FEA reflects the real-world scenarios. The following constraints and assumptions are

applied.

Thermal boundary conditions:

The reference temperature is set to 20 °C throughout the entire simulation process,

which typically represents the laboratory ambient temperature.

Heat source (Tool tip temperature): a constant temperature is applied at the cutting tip

based on the values from DOE for each simulation.

Ambient Temperature: The tool body is exposed to atmospheric conditions with a fixed

ambient temperature as one of the continuous input parameters in the DOE. This

boundary condition is used to simulate convective heat transfer from the tool's surface,

which is exposed to the environment. Convective heat transfer between the tool holder

and clamp is also considered for the simulation to more accurately represent the thermal

interaction at their interface.

LN₂ cooling interface: The internal surfaces of the expansion chamber and coolant

channels are subjected to convective cooling using LN₂. The heat transfer coefficient for

LN₂ is defined parametrically and varied in the simulation as per DOE settings.

Structural boundary conditions:

Fixed support: the tool shank is constrained as a rigid to be clamped in the tool holder

for the simulation.

Load application: Experimental values obtained from lab tests are used to apply realistic

machining forces. The following constant loads are applied at the tool tip:

Feed Force (F_f): 150 N

Cutting Force (F_c): 50 N

Peripheral Force (F_N) : 50 N

These forces are applied directionally to reflect actual hard turning conditions.

Contact interface: Interfaces such as insert support-tool head, tool head-shank, cutting

insert - Insert support, and insulation pad-shank are defined with bonded contact

settings to simulate heat and stress transfer between components. This assumption

28

implies that there is no relative motion or separation between these surfaces, ensuring the continuous transfer of both heat and mechanical stress across the interfaces. Bonded contact is suitable where the primary focus is on overall heat and stress distribution through rigidly connected parts [61].

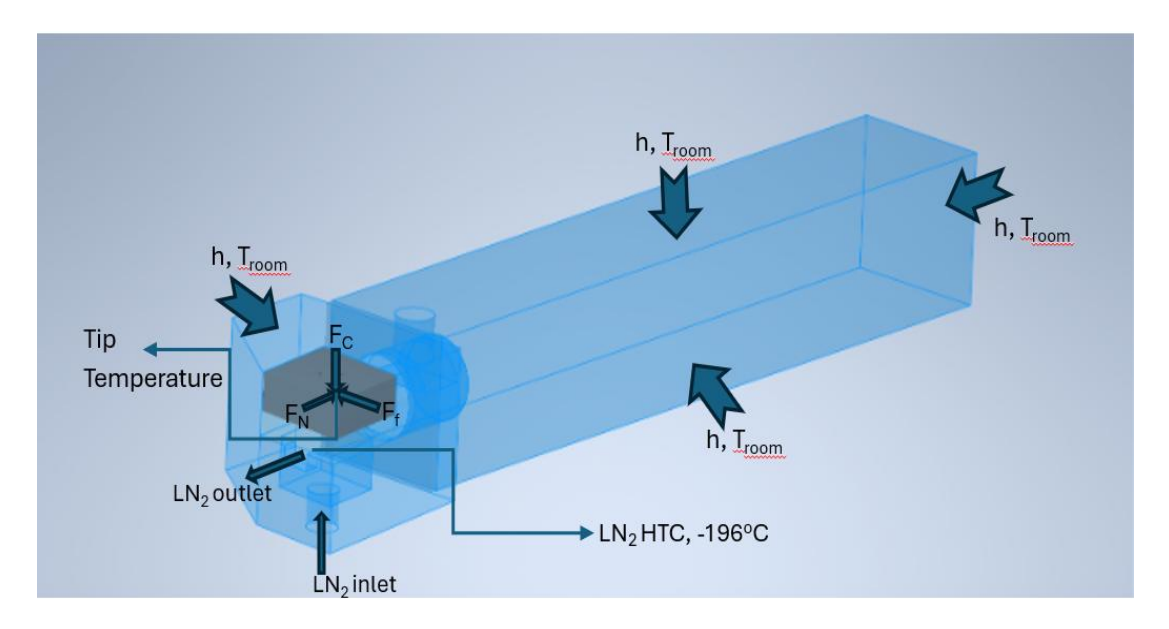


Figure 3.6 : Boundary conditions of the model.

3.3.4. Simulation types

To verify and optimize the performance of the proposed turning tool with an internal cooling chamber, two finite element methods (FEM) will be conducted using ANSYS Workbench 2024 R2. The two finite element simulations are a steady-state thermal analysis and a static structural analysis. These simulations are very important in evaluating thermal behaviour and mechanical integrity of the design, especially under machining conditions that involve extreme thermal and mechanical loadings.

Steady-state thermal analysis

In steady-state thermal analysis temperature field is evaluated over the fixed conditions. The governing principle for this kind of simulation is Fourier's Law of Heat Conduction, which states that heat flux is directly proportional to the negative temperature gradient.

$$q = -k\nabla T \tag{3.2}$$

where k is the thermal conductivity [62]

Then, by applying conservation of energy and enforcing steady state conditions, $(\partial T/\partial t=0)$, the Eulerian steady-state heat conduction equation is derived as:

$$\nabla * (k\nabla T) = 0 \tag{3.3}$$

The above formula indicates that the net heat flux into any fixed spatial region is zero. This method is advantageous for this project because boundary conditions can be directly and precisely imposed on the stationary mesh. The resulting temperature loads serve as a critical input for downstream structural and thermo-mechanical analyses, thus forming a cohesive and efficient simulation workflow.

Static structural analysis

In static structural analysis, the mechanical behaviour of the tool, such as stress and deformation, is evaluated under time-invariant loading, combining cutting forces and thermal loads due to cryogenic and cutting temperature conditions. The purpose of this analysis is to ensure the tool's structural integrity and dimensional stability under operational conditions.

The analysis is grounded in the fundamentals of equilibrium of internal and external forces. Stress is expressed by the Cauchy equation [63].

$$\sigma = \begin{bmatrix} \sigma_{xx} & \tau_{xy} & \tau_{xz} \\ \tau_{yx} & \sigma_{yy} & \tau_{yz} \\ \tau_{zx} & \tau_{zy} & \sigma_{zz} \end{bmatrix}$$
(3.4)

Where σ is the Cauchy stress tensor. The stress and strain relation (Hook's Law) is as given in equation 4.5 below

$$\begin{bmatrix} \varepsilon_{x} \\ \varepsilon_{y} \\ \varepsilon_{z} \\ \gamma_{xy} \\ \gamma_{yz} \\ \gamma_{zx} \end{bmatrix} = \frac{1}{E} \begin{bmatrix} 1 & -\nu & -\nu & 0 & 0 & 0 & 0 \\ -\nu & 1 & -\nu & 0 & 0 & 0 & 0 \\ -\nu & -\nu & 1 & 0 & 0 & 0 & 0 \\ 0 & 0 & 0 & 2(1+\nu) & 0 & 0 & 0 \\ 0 & 0 & 0 & 0 & 2(1+\nu) & 0 & 0 \\ 0 & 0 & 0 & 0 & 0 & 2(1+\nu) \end{bmatrix} \begin{bmatrix} \sigma_{x} \\ \sigma_{y} \\ \sigma_{z} \\ \tau_{xy} \\ \tau_{yz} \\ \tau_{zx} \end{bmatrix}$$
(3.5)

Strain displacement relations, which are given below Eq. (3.6)-(3.11), describe how the displacement gradient gives rise to strain [63].

$$\varepsilon_{x} = \frac{\partial_{x}}{\partial_{u}} \tag{3.6}$$

$$\varepsilon_{y} = \frac{\partial_{y}}{\partial_{v}} \tag{3.7}$$

$$\varepsilon_{z} = \frac{\partial_{z}}{\partial_{w}} \tag{3.8}$$

$$\gamma_{xy} = \frac{\partial_x}{\partial_y} + \frac{\partial_y}{\partial_y} \tag{3.9}$$

$$\gamma_{yz} = \frac{\partial_w}{\partial_y} + \frac{\partial_v}{\partial_z} \tag{3.10}$$

$$\gamma_{zx} = \frac{\partial_u}{\partial_z} + \frac{\partial_w}{\partial_x} \tag{3.11}$$

The equilibrium equations Eq. (3.12)-(3.14) ensure that the internal stresses balance the external forces applied to the body [63].

$$\frac{\partial \sigma_{xx}}{\partial_x} + \frac{\partial \tau_{xy}}{\partial_y} + \frac{\partial \tau_{xz}}{\partial_z} + x = 0$$
(3.12)

$$\frac{\partial \tau_{xy}}{\partial_x} + \frac{\partial \sigma_{yy}}{\partial_y} + \frac{\partial \tau_{yz}}{\partial_z} + Y = 0$$
 (3.13)

$$\frac{\partial \tau_{xz}}{\partial_x} + \frac{\partial \tau_{yz}}{\partial_y} + \frac{\partial \sigma_{zz}}{\partial_z} + Z = 0$$
 (3.14)

Where, X, Y, and Z are body forces in the respective directions.

The governing equation of elasticity in vector form (Navier's equation) can be written as:

$$(\lambda + G)\frac{\partial_e}{\partial_x} + G\nabla^2 u + X = 0$$
(3.15)

Where λ and G are Lamé's constants. The volumetric strain is given by:

$$e = \varepsilon_{xx} + \varepsilon_{yy} + \varepsilon_{zz} + \frac{\partial_u}{\partial_x} + \frac{\partial_v}{\partial_y} + \frac{\partial_w}{\partial_z}$$
(3.16)

In this study, the finite element method (FEM) will be employed using ANSYS Workbench to solve the above equations numerically. The tool holder geometry will be meshed, boundary conditions will be applied, and material properties will be defined for different tool head materials. The analysis outputs include total deformation and Von Mises stress distribution, which help in evaluating the feasibility of each design under operational conditions.

Chapter 4

Results and discussion

In this chapter, the results obtained from the numerical simulations and the statistical analysis for the proposed cryogenic cooling concept of a turning tool with an integrated LN₂ chamber are presented. The primary objective of the study was to evaluate the thermal and structural performance of the tool under the applied loads and cryogenic conditions and to identify the influence of key parameters using response surface methodology (RSM). To achieve these objectives, ANSYS was utilized to conduct steady-state thermal analysis and static structural analysis, focusing on temperature distribution, stress concentration, and deformation within the tool body.

After the simulation, RSM is used to analyse the effect of the selected input parameters, namely LN_2 heat transfer coefficient, tool tip temperature, ambient temperature, insulation mechanism, and the chamber size on the thermal performance and structural stability of the tool.

4.1. Simulation results

4.1.1. Thermal analysis results

Temperature distribution results for the variant with insulation coating in the chamber

Based on the DOE matrix arrangement, a total of 80 simulations were carried out using ANSYS Workbench to analyze the thermal behavior of the tool with an integrated internal cooling chamber under cryogenic conditions. The key parameters were arranged carefully, and material properties were assigned to all the parts. One of the initial configurations, shown in Figure 4.1, corresponds to the variant with coating the LN_2 chamber as an insulation method, a smaller size of the chamber, and a heat transfer coefficient of $40,000W/(m^2.K)$ for this configuration. the tip temperature was considered to be $450\,^{\circ}\text{C}$ while the ambient temperature was maintained at $22.5\,^{\circ}\text{C}$.

The thermal analysis result presented in Figure 4.1 clearly shows the impact of cryogenic cooling on the temperature distribution. The comparison between cryogenic cooling (Figure 4.1a and c) and dry cutting conditions (Figure 4.1b and d) show important information regarding the heat accumulation, thermal gradient, and effectiveness of the cryogenic cooling during machining.

Under the dry cutting conditions, the tool exhibits high temperature concentrations near the cutting tip and insert area, indicating poor heat dissipation. This heat concentration poses a significant risk for tool wear, thermal softening, and dimensional instability during prolonged cutting operations. The sectional view (Figure 4.1d) shows that the heat is trapped from the cutting insert and insert support with minimal heat flow or convection due to the absence of cooling.

In the cryogenic cooling case (Figure 4.1a and c) show an improved thermal profile with more gradual temperature distribution along with the cutting tool.

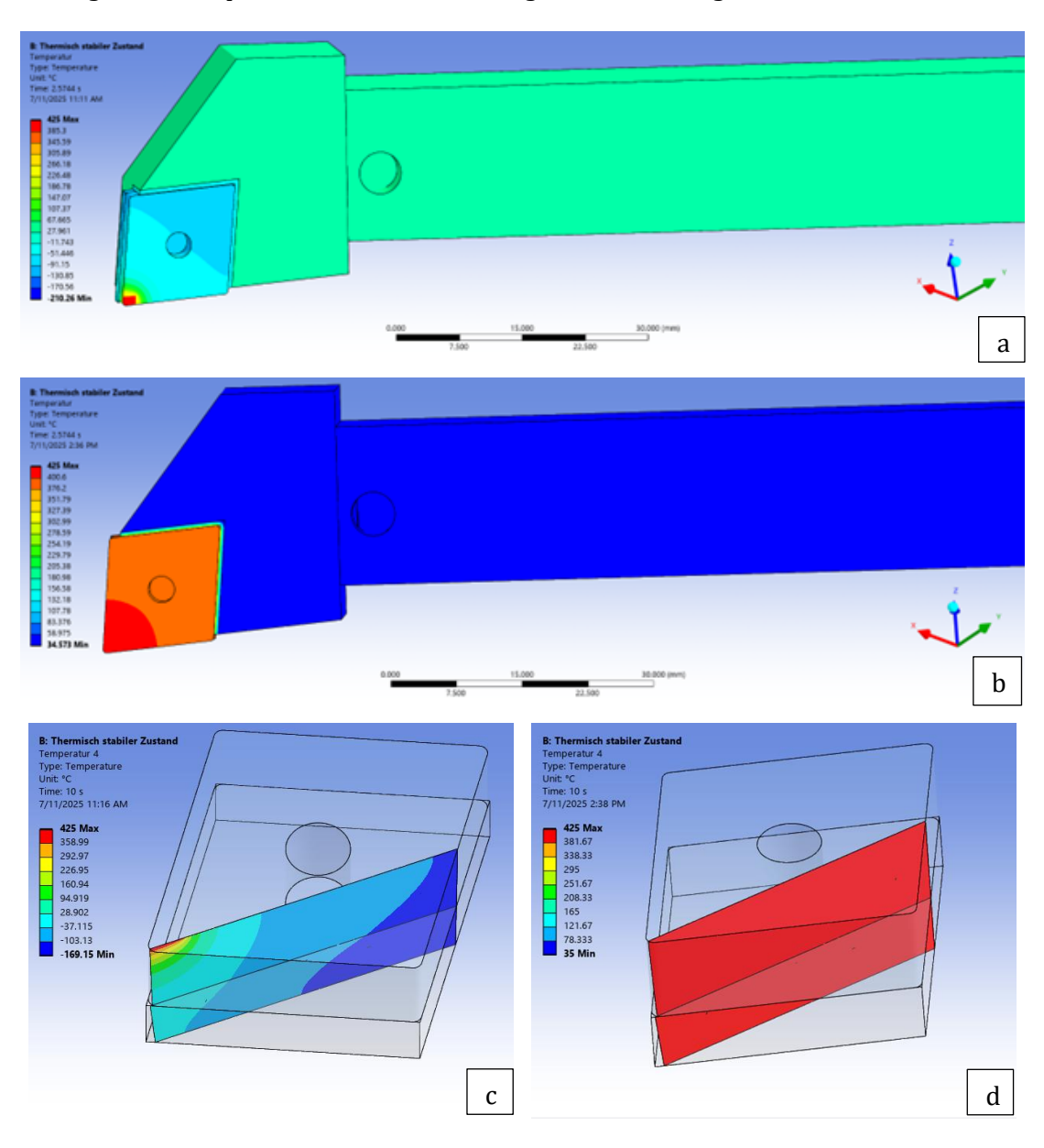


Figure 4.1: Temperature distribution results from steady state thermal simulation of the internally cooled turning tool: a) cutting tool under cryogenic cooling conditions, b) temperature distribution of the tool under dry conditions, c) sectional view under cryogenic cooling, d) sectional view under dry conditions.

The effect of the cryogenic cooling on the thermal effect compared to the dry one can be summarized in Figure 4.2 below, which shows the temperature distribution along the selected path through the diagonal of the cutting insert and the tool head.

Figure 4.2a and b present the result of the thermal simulation along the defined diagonal path of the cutting tool under cryogenic cooling using liquid nitrogen and dry cutting, respectively. The plot in Figure 4.2c illustrates the corresponding temperature values as a function of distance from the tool tip.

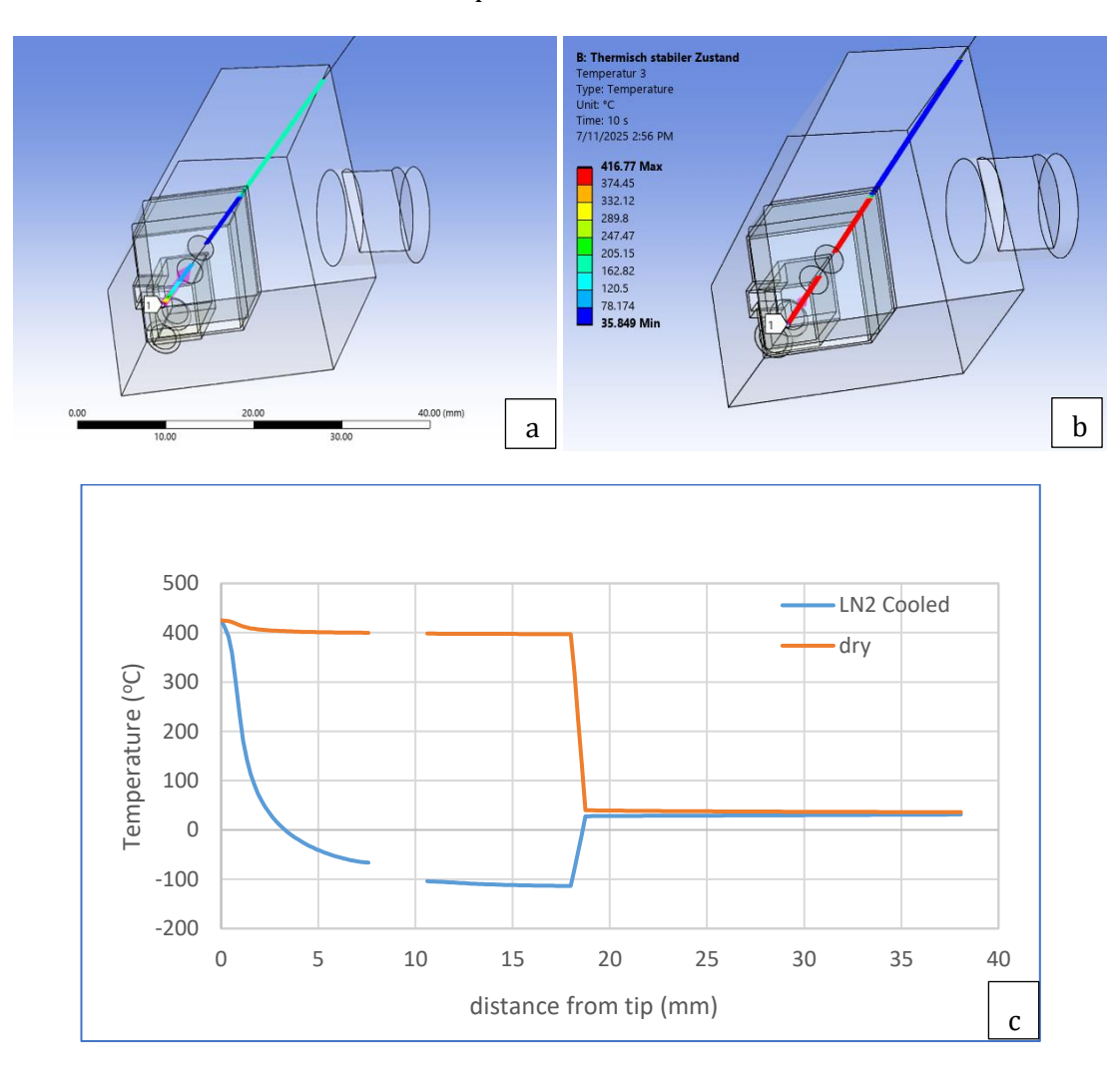


Figure 4.2 : Temperature distribution along the diagonal path, a) cryogenically cooled tool, b) dry machining. c) graph for the temperature distribution of the dry and cryogenically cooled tool.

The result shows the rapid heat dissipation occurring within the first few millimeters along the path, indicating the efficient heat extraction under liquid nitrogen-cooled conditions. Conversely, for the tool without LN₂ cooling, the thermal energy remains concentrated in the region near the cutting tip with an elevated temperature extending through the cutting insert's whole body. The reduced thermal gradient indicates ineffective heat dissipation and greater thermal loading on the tool.

An important aspect observed in both the simulation results is the effect of the insulation coating applied to the liquid nitrogen chamber. In both cases, the insulation coating appears to effectively limit the propagation of heat from the cutting insert to the tool head. This is evident from the graph for the LN_2 -cooled case, where the temperature drops dramatically and remains suppressed beyond a certain distance, confirming that the coating helps to localize the cooling effect at the cutting zone, in addition to enhancing thermal isolation.

Temperature distribution result for the model with an insulation pad between the tool head and the tool shank.

In the second variant, where an insulation pad is utilized between the tool head and the tool shank, but no insulation coating was applied to the walls of the LN_2 chamber, different thermal behaviour was observed compared to the initial model. The boundary conditions, such as chamber geometry, LN_2 heat transfer coefficient, tool tip temperature, and atmospheric temperature, were maintained the same to ensure the direct comparison. Unlike the previous case, where the chamber was coated, which effectively restricted heat propagation through the tool head, the absence of an insulation coating in this case allowed more heat dissipation throughout the whole tool head. Consequently, the insulation pad between the tool head and tool shank restricts the heat flow into the shank. This led to a broader temperature distribution, where the heat introduced at the cutting insert not only affected the immediate zone of the cutting insert but also spread through the tool head. The corresponding temperature distribution for this configuration is included in Figure 4.3 below, showing the influence of the presence of the insulation coating of the LN_2 chamber on the temperature distribution throughout the tool head.

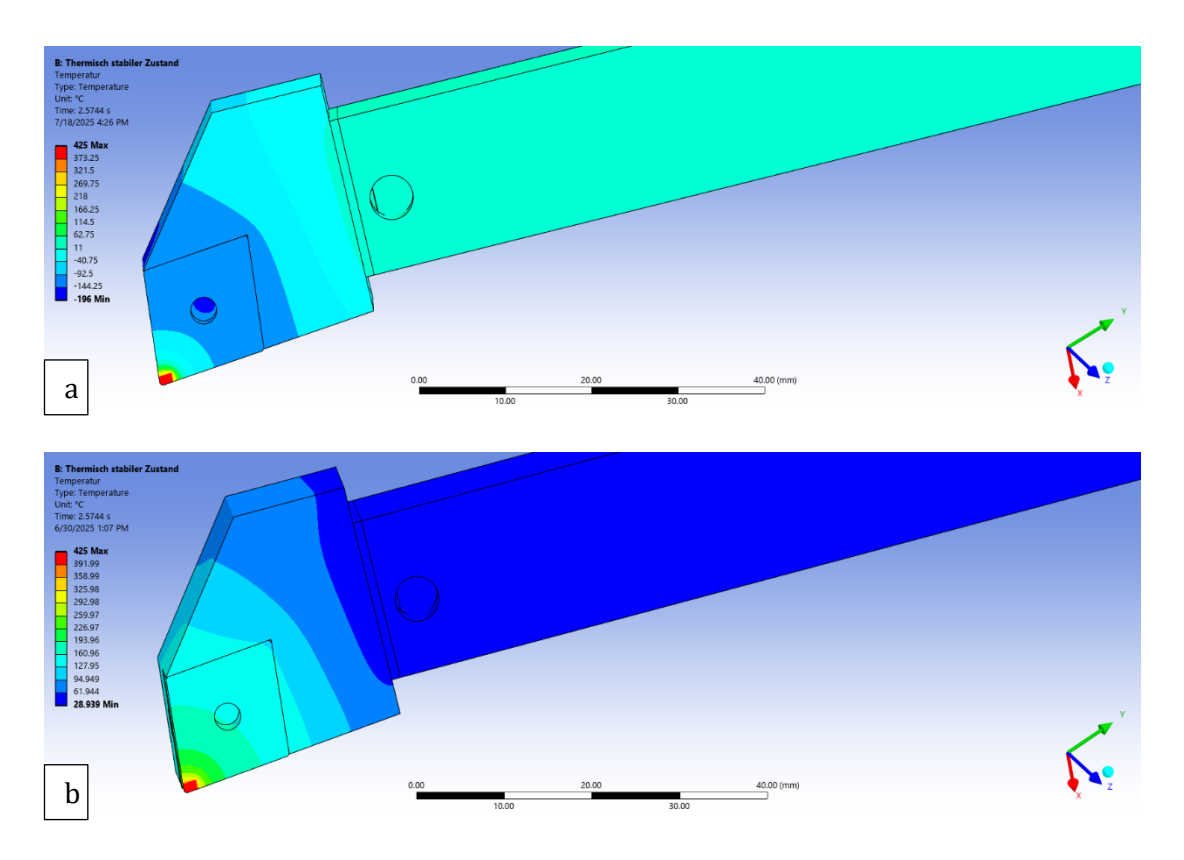


Figure 4.3: Temperature distribution along the tool holder length for the model with an insulation pad between the tool head and shank. A) cooled by LN₂, b) dry machining.

The graph below in Figure 4.4 shows the temperature distribution along the diagonal path of the tool for the tool with an insulation pad between the head and the tool shank under dry conditions and liquid nitrogen cooling. As a boundary condition, the tool tip temperature was set to 425 °C, heat transfer coefficient 40,000W/(m²·K), and atmospheric temperature 22.5 °C.

In the dry machining Figure 4.4b, the heat penetrates into the tool head, and the temperature remains high along the insert body and also indicating the heat conduction into the tool assembly, which could negatively affect the thermal stability and tool life. In contrast, in the cryogenically cooled condition (Figure 4.4a), the temperature profile exhibits a steep gradient, with heat dissipating rapidly from the tool tip. Most of the cutting insert region remains close to ambient and below zero due to the cryogenic cooling, showing the effectiveness of the cryogenic cooling system.

The graph in Figure 4.4c provides a direct comparison of the temperature distribution along the diagonal path for the configuration with an insulation pad between the tool head and shank. Under dry conditions, the temperature decreases gradually but remains significantly above the ambient, indicating the wider spread of heat throughout the tool. In the LN₂-cooled case, a sharp temperature drop within the first few millimeters from

the cutting tip was observed, and the cryogenic cooling effect continues throughout the tool head.

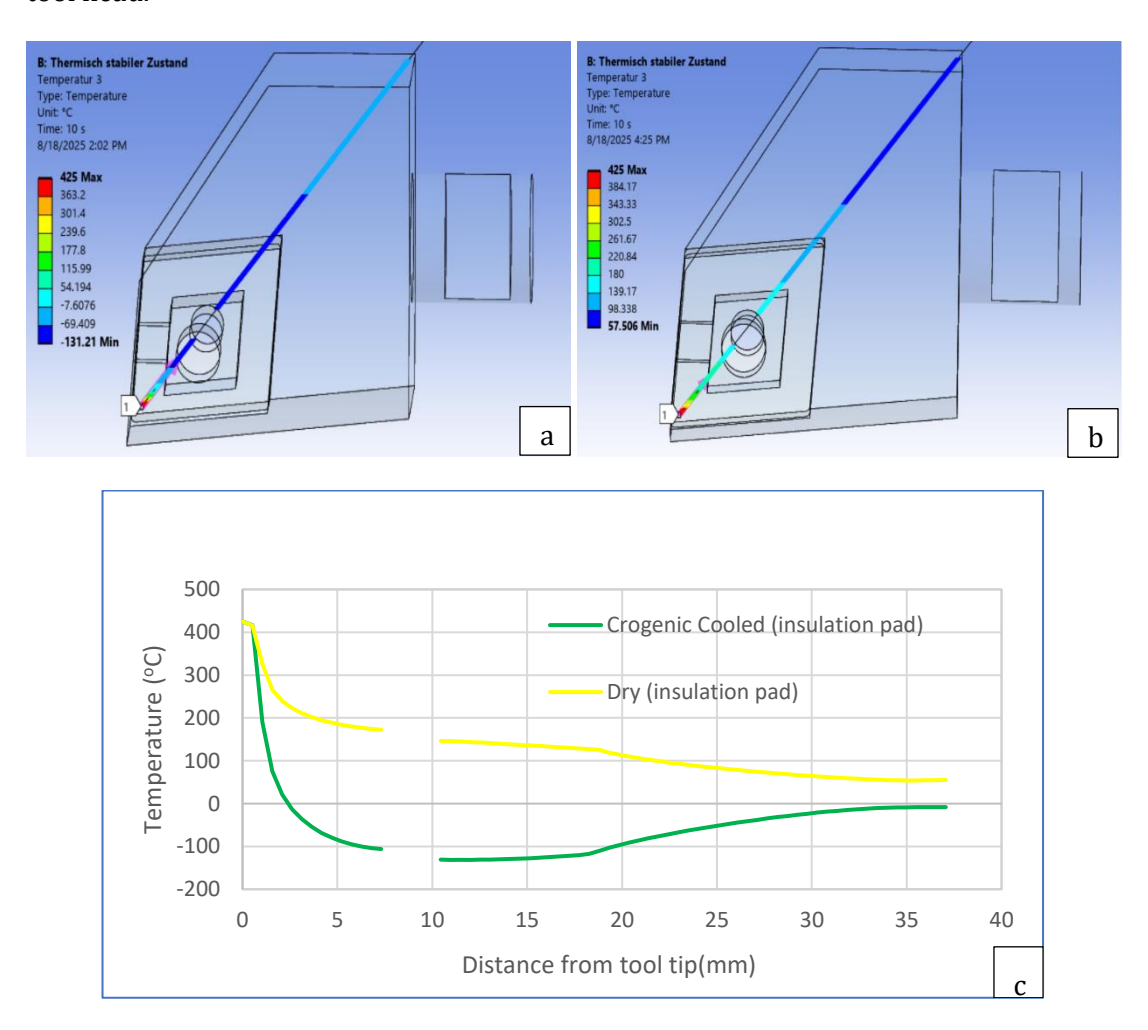


Figure 4.4: Temperature distribution along the diagonal path for the configuration with an insulation pad between head and shank, a) cryogenically cooled tool, b) dry machining. c) graph for the temperature distribution of the dry and cryogenically cooled tool.

The thermal analysis in this study was primarily run under the steady-state conditions for all tool configurations. To further assess the steady state thermal analysis and to understand the heat propagation process, a transient thermal simulation was also performed for a single representative model. The configuration with chamber coating was chosen, and a transient simulation was run using the same geometry, material properties, and boundary conditions as the steady-state case: tip temperature of 425 °C, Heat Transfer coefficient (HTC) of 40,000 W/(m^2 .K), and atmospheric temperature of 22.5 °C. However, due to the element count limitation of the ANSYS student version, a coarser mesh was adopted for the transient simulation.

The transient results, shown in Figure 4.5, present the temperature-distance profiles at various time steps (t = 10s, 30s, 60s, 100s, 110s, 130s, and 150s) along the diagonal path through the cutting insert. At the initial time steps (t = 10s, 30s, and 60s), the result shows a steep temperature gradient along the path. As time progresses, the temperature distribution throughout the cutting insert becomes almost identical after t = 100sec, closely resembling the steady state profile. The visible discontinuous gap in the graph is due to the geometric construction of the tool.

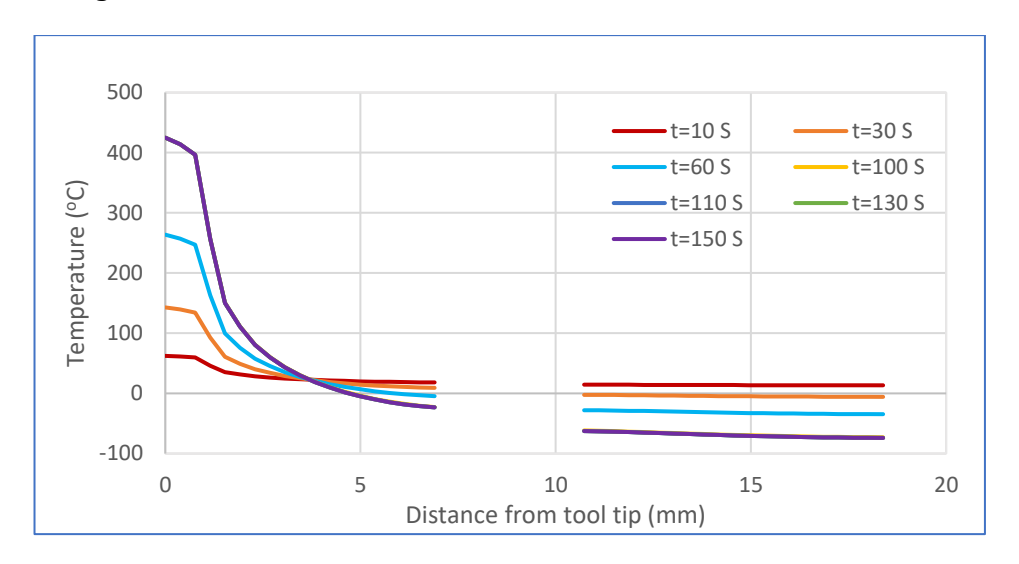


Figure 4.5 : Temperature distribution along the diagonal path through the cutting insert at different time intervals.

The temperature–time graph in Figure 4.6 indicates the variation of maximum, minimum, and average temperatures throughout the simulation. In the early stage, the maximum temperature increases rapidly until the maximum tip temperature set is reached, while the minimum temperature reduces as the cooler region of the tool approaches the thermal balance. The average temperature remains relatively stable throughout the process, reflecting gradual thermal equalization throughout the tool. Both maximum and minimum temperature stabilizes and plateau after approximately 100 seconds.

The transient simulation confirms that under specified operating conditions, the system achieves steady state behavior within roughly 100 seconds. The convergence of the temperature-time curves towards stable values after some simulation period confirms that the assumptions of steady-state thermal conditions in the DOE framework for this research can be considered representative of the thermal behavior of the tool during machining.

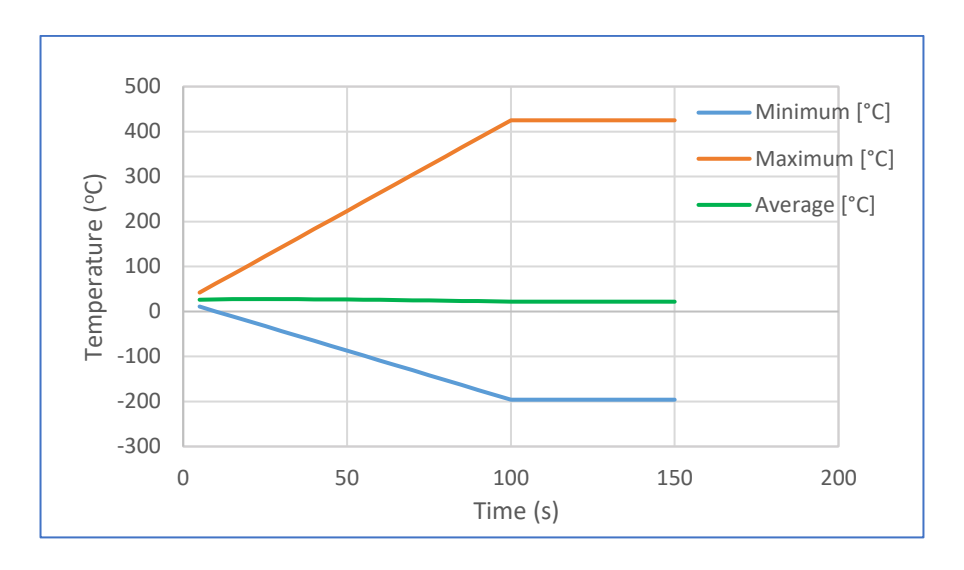


Figure 4.6 : Time evolution of maximum, minimum, and average temperatures.

Figure 4.7 presents the temperature distribution along the diagonal path of the tool head under different configurations, and it is observed that the chamber-coated configuration provides a more localized cooling effect concentrated around the cutting insert. In contrast, the configuration with an insulation pad between the tool head and shank provides a cooling effect throughout the tool head. It is also observed that the transient simulation follows the same structure as the steady state distribution under the same configurations and boundary conditions.

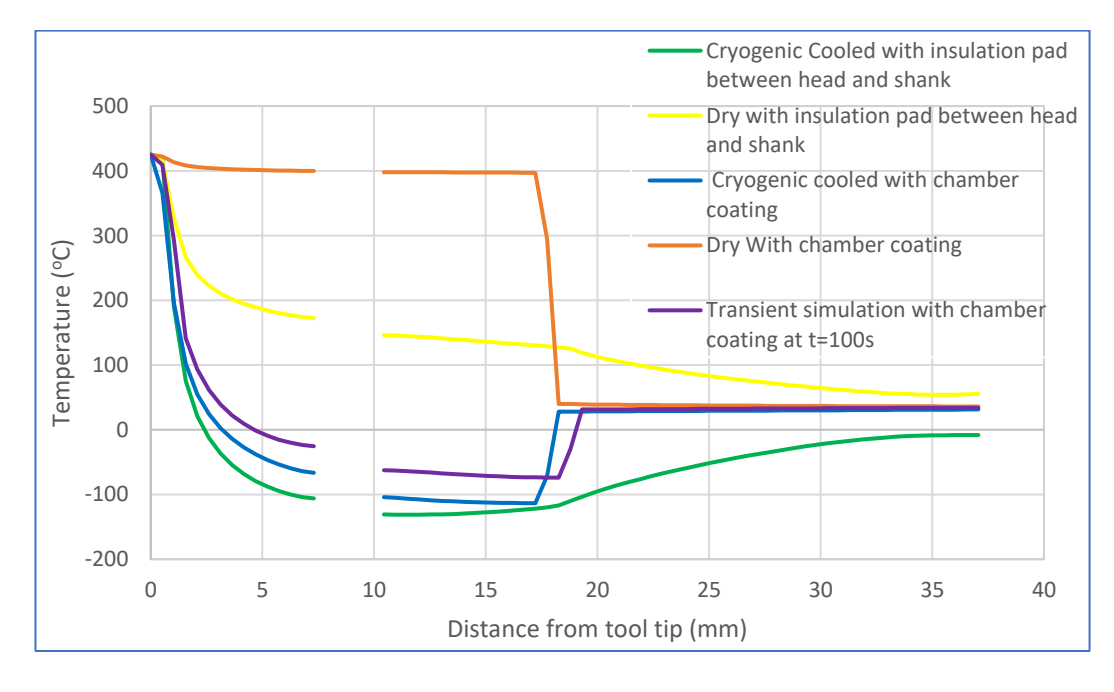


Figure 4.7 : Temperature distribution along the diagonal path of the tool for different configurations.

4.1.2. Structural analysis results

The static structural analysis was performed to evaluate the structural stability of the turning tool under the applied mechanical loads and thermal loading conditions obtained from the steady state thermal analysis. The objective is to assess the stress distribution and the deformation of the tool under the applied conditions.

Figure 4.8 shows the result from the structural analysis, which incorporated the thermal loading results from the steady state thermal analysis conducted using a heat transfer coefficient (HTC) of 40,000W/(m².K), a tool tip temperature of 425 °C, and an ambient temperature of 22.5 °C. The plot illustrates Von-Mises stress distribution throughout the tool assembly. The maximum equivalent stress is observed at the cutting insert seat region, with a peak value of 408.48MPa. this region corresponds to the contact interface between the cutting insert and the workpiece material, where both mechanical and thermal loads are highly concentrated. High stress concentration at the cutting insert seat is expected due to the direct application of the cutting forces and steep thermal gradient in this area.

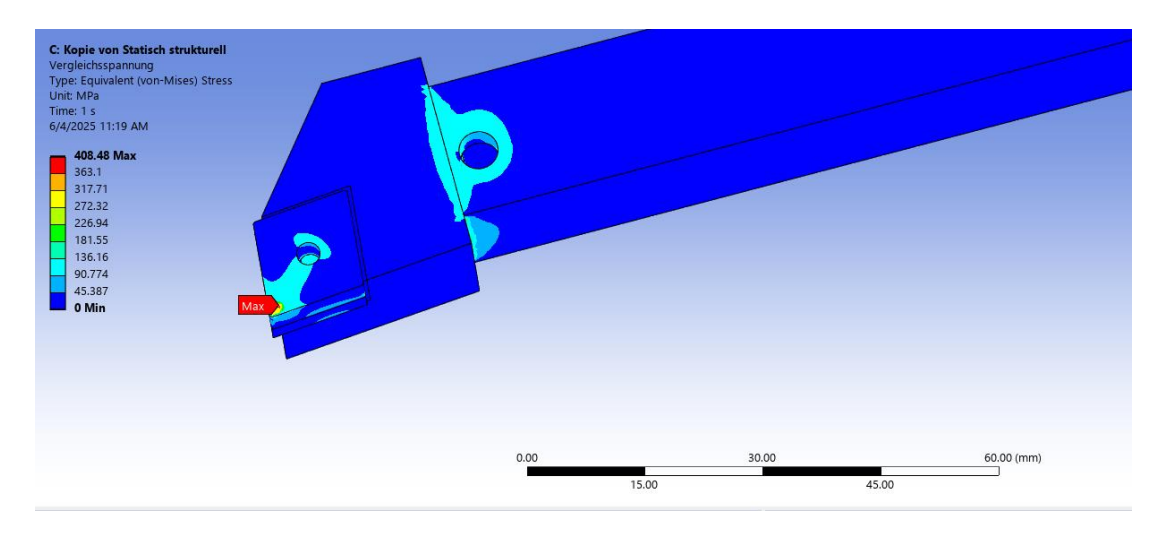


Figure 4.8 : Stress distribution through the tool under cryogenic cooling conditions for the tool variant with insulation coating in the LN_2 chamber.

To assess the structural stability of the designed tool, the factor of safety was calculated using the maximum equivalent Von Mises stress obtained from the structural analysis and the yield stress of the tool head material (AISI H13 Tool steel)

$$FOS = \frac{yield\ stress}{design\ stress}$$

$$FOS = \frac{1200MPa}{408.48MPa}$$

$$= 2.937$$
(4.1)

The calculated factor of safety value indicates that the designed tool can reliably withstand the applied loads under the specified conditions [64].

In Figure 4.9 below, the equivalent Von Mises stress distribution for the tool assembly model in the configuration where the insulation pad is integrated between the tool head and the shank. The simulation reveals a significant increase in the stress compared to the tool assembly with an insulation coating in the chamber of LN_2 , with the maximum stress reaching 1009.5MPa.

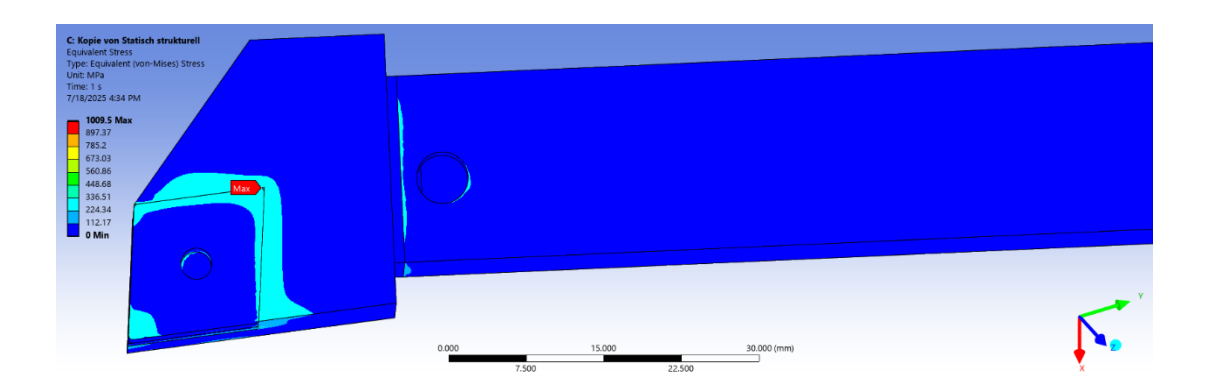


Figure 4.9: stress distribution through the tool under cryogenic cooling conditions for the tool variant with an insulation pad between the tool head and shank.

From the static structural analysis result, it is observed that the insulation method has a great impact on the tool design. In the model with configuration in which the insulation coating is applied in the chamber of the LN_2 lower stress value than the model with insulation pad between the head and shank. This difference is attributed to the localized and effective cooling in the first variant, where the insulation coating isolates the cryogenic flow to the tool head. this ensures the cooling effect near the cutting insert and immediate support, as a result thermal gradients are reduced, and stress concentration is lower across the tool.

Comparison of the maximum Von Mises stress in the tool is presented in Figure 4.10 across four different configurations, under identical boundary conditions (Heat transfer coefficient (HTC) of $40,000W/(m^2.K)$, Atmospheric temperature of 22.5 °C, and tip temperature of 425 °C). As it is indicated in Figure 4.10, the LN_2 -cooled configuration

with chamber coating resulted in the lowest stress level, where the stress remained below 420MPa. This result underscores the effect of cryogenic cooling in limiting thermal stress across the tool by dissipating heat. In contrast, the configuration with dry conditions and chamber coating resulted in the highest stress response, exceeding 1100MPa, which resulted from a lack of active cooling.

When an insulation pad is introduced at the tool head and shank interface, it is discovered that the maximum stress is slightly increased, indicating that the insulation method has a major effect on the designed tool structural stability, and chamber coating is more effective in mitigating the stress.

The dry condition with an insulation between the tool head and the shank reduces the stress compared to the same condition under a chamber coating case. This suggests that introducing the insulation between the tool head and shank offers some heat dissipation across the tool head instead of localized high-temperature heating.

Generally, the result clearly demonstrates that the integration of liquid nitrogen cooling with chamber insulation coating minimizes the stress by providing localized, efficient cooling.

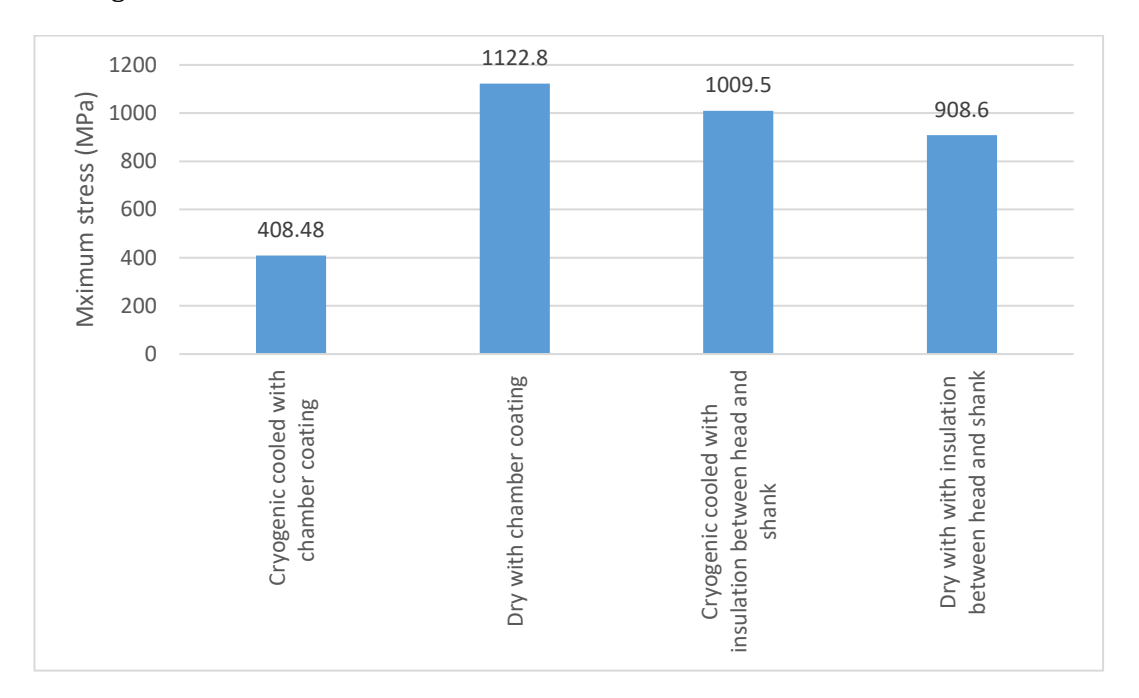


Figure 4.10: Maximum Von Mises stress on the tool under different conditions.

The deformation results from the static structural analysis for the tool variant with two different insulation method is illustrated in the Figure 4.11 below. In both cases thermal loads from steady state thermal analysis (HTC = $40,000 \text{ W/(m}^2 \cdot \text{K})$, tool tip temperature = 425°C , ambient temperature = 22.5°C) were used, combined with mechanical forces replicating hard machining conditions.

The maximum deformation for the variant with insulation coating in the LN_2 chamber is observed to be 0.037mm (Figure 4.11a), which is lower than the maximum deformation for the tool with an insulation pad between the head and shank, 0.0419mm. this demonstrates that the structural stability of the tool assembly is improved when insulation is directly applied to the LN_2 chamber instead of inserting an insulation pad between tool components. This is also mainly attributed to the localized cooling around the insert and insert support, which is achieved by effective containment of cryogenic temperature within the chamber region.

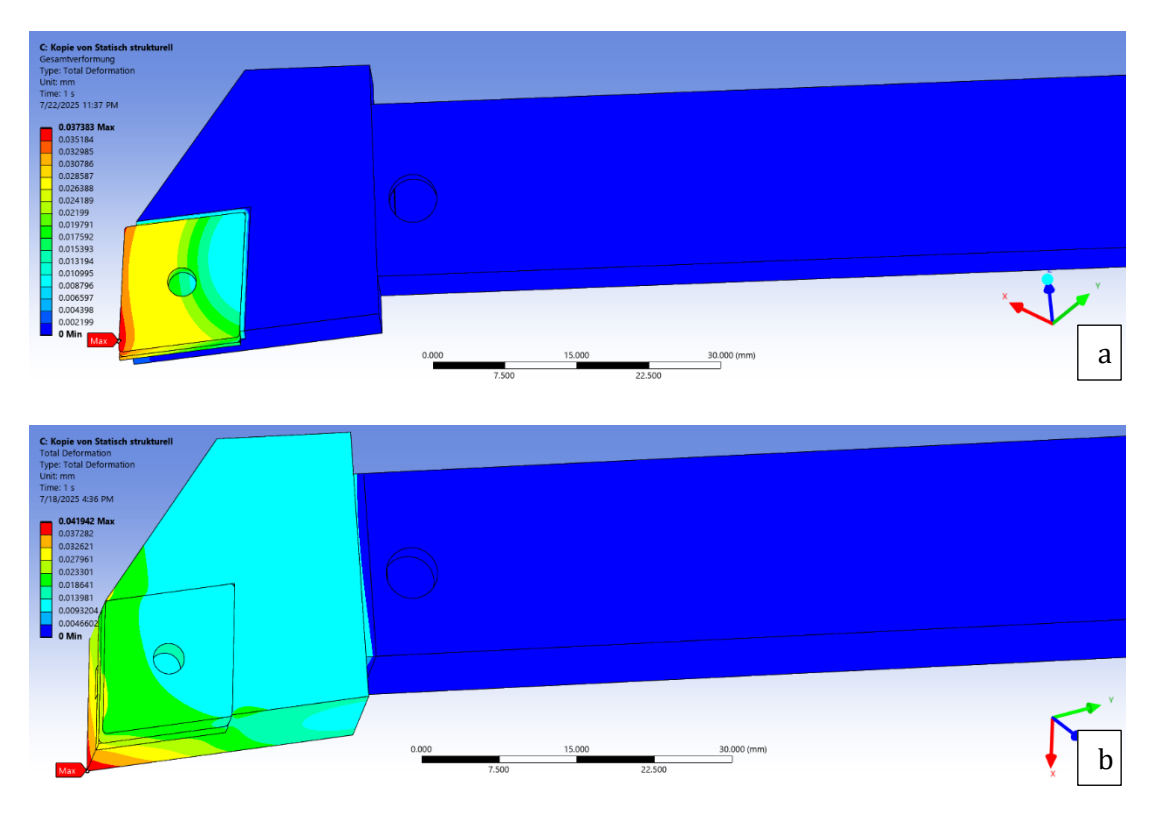


Figure 4.11: Total deformation throughout the tool a) tool with insulation coating in the chamber, b) variant with an insulation pad between the tool head and shank.

Results of maximum stress and maximum deformation for all the simulations under different combinations of the parameters are provided in Appendix A.

4.1.3. Effect of the tool head material on the structural stability

To assess the structural stability of the tool design across different material selections, a series of structural simulations were carried out for five different candidate materials for the tool head from the material selection. The simulations were run under identical conditions, including the thermal load derived from the steady state thermal analysis $(HTC = 40,000W/(m^2.K))$, tip temperature = 425 °C, ambient temperature = 22.5 °C) and mechanical forces representative of hard machining operations.

Figure 4.12a shows the comparison of maximum Von Mises stress values of the designed tool for different tool head materials, showing that the proposed candidate materials for the tool head demonstrate similar stress resistance under the applied conditions, with a difference in maximum stress negligible (less than 0.1MPa). This suggests that the material selection among the selected candidates has a minor influence on the stress distribution.

Similarly, Figure 4.12b presents total deformation along the tool for different materials, which also remains constant across all the proposed candidate materials. The variation in total deformation across the tool throughout all the proposed materials is minimal.

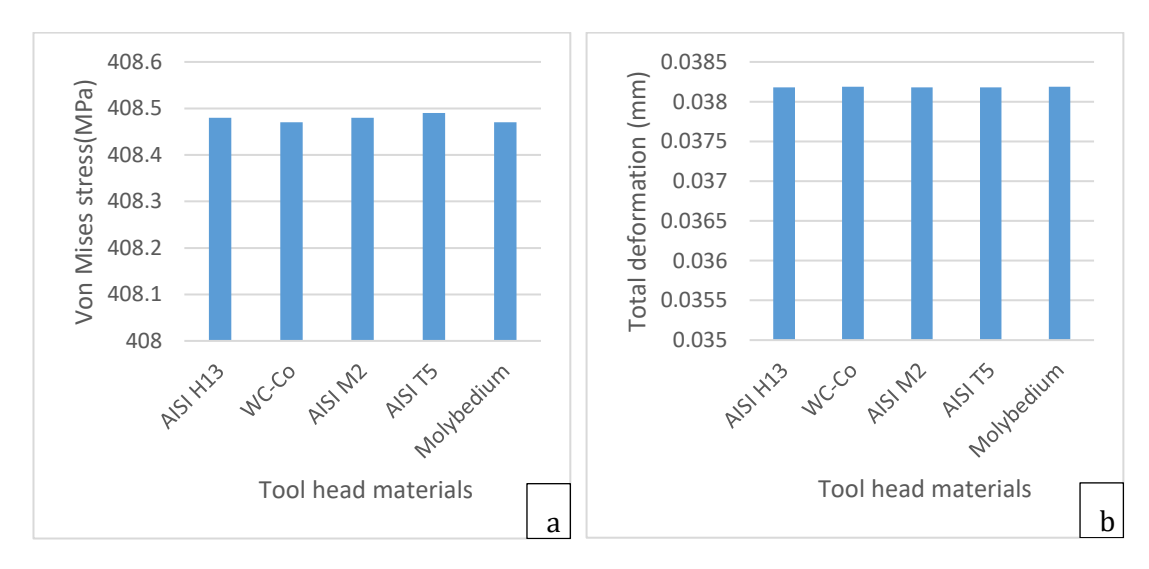


Figure 4.12: a) maximum stress for different tool head materials under identical conditions, b) maximum deformation for different tool head materials under identical conditions.

4.2. Parametric analysis of key factors

To understand the influence of the key parameters on the structural behavior of the designed tool under cryogenic conditions, a parametric analysis was performed using the response surface method (RSM). A total of 80 simulation orders were generated based on a design of experiment (DOE) matrix. For each simulation, a steady-state thermal analysis was run, followed by a static structural analysis using the results from the thermal analysis as input.

The analysis was based on the finite element simulations (FEM), and the primary input parameters included in the DOE matrix were: LN_2 heat transfer coefficient, chamber size, insulation method, tool tip temperature, and environmental temperature.

4.2.1. Model adequacy and ANOVA results

To assess the suitability of models, influential variables, and parameter interactions, the analysis of variance (ANOVA) is frequently used for both stress and maximum deformation. ANOVA can also be employed to validate the predictive models [65]. Using Minitab software, an ANOVA was performed according to the simulation results of the maximum Von Mises stress and maximum deformation from the static structural simulation. The ANOVA findings for Maximum stress and maximum deformation are shown in Table 4.1 and Table 4.2.

Model summaries for both stress and deformation are shown in Figure 4.13 below. As indicated in Figure 4.13, the model summary shows that the model exhibited an excellent fit for both maximum stress and maximum deformations. The standard deviation (S) value for the maximum stress model is due to the range of the maximum stress values, which is several hundred MPa.

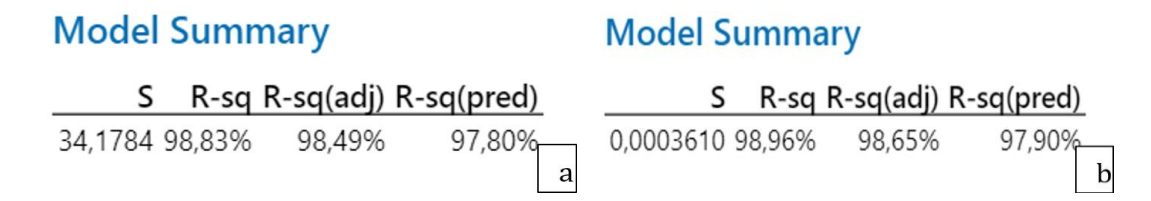


Figure 4.13 : Model summary a) maximum stress model, b) maximum deformation model.

Typically, it is assumed that the model, influential variables, and their interactions are considered statistically significant when the p-value for the 95 percent confidence interval is less than 0.05 [65].

According to the above criteria, the P-value for both stress and deformation models is less than 0.05, as indicated by the ANOVA results, suggesting that the models are statistically significant.

The residual analysis further confirms that the regression model developed for predicting maximum deformation and maximum stress is adequate. The normal probability plot shows the residuals are almost linearly distributed along the diagonal, indicating that the errors are approximately normally distributed. The histograms of the residuals also support the assumptions for normality. In the residual versus fitted values plot, the residuals are randomly scattered, implying the absence of autocorrelation in the simulation order. The residual analysis in Appendix B supports the validity of the regression model used in the response surface methodology.

The regression equations for both maximum stress and maximum deformation are provided in Appendix C for all the configurations of the models.

The ANOVA results for the stress model, presented in Table 4.1, reveal that several parameters have a statistically significant influence on the response. Among the linear factors, the heat transfer coefficient (HTC), tip temperature, chamber size, and insulation method exhibited highly significant effects with P-values below 0.05, which indicates the strong individual contributions to the stress concentration behavior. In contrast, atmospheric temperature showed an insignificant effect (P-Value = 0.845), suggesting minimal direct impact on stress concentration in the simulated conditions.

In addition, several two-way interactions were identified to be significant. These include HTC × insulation method, tip temperature × chamber size, tip temperature × insulation method, and chamber size × insulation method. These findings emphasize the complex interdependence between design and cooling parameters in determining the structural behavior of the tool. On the other hand, Interactions involving atmospheric temperature and HTC with other variables were found to have an insignificant effect.

Similarly, ANOVA results for the maximum deformation model presented in Table 4.2 show that heat transfer coefficient (HTC), tip temperature, chamber size, and insulation method contribute significant effects on the maximum deformation values throughout the tool with P-values below 0.05, while atmospheric temperature showed an insignificant effect with P-value 0.232. The two–way interactions such as HTC \times insulation method, tip temperature \times chamber size, tip temperature \times insulation method, and chamber size \times insulation method are also found to be significant.

					P-
Source	DF	Adj SS	Adj MS	F-Value	Value
Model	18	6044891	335827	287.48	0.000
Linear	5	5732496	1146499	981.45	0.000
HTC	1	10875	10875	9.31	0.003
Atm. Temperature(oC)	1	45	45	0.04	0.845
Tip Temperature	1	150	150	0.13	0.721
chamber size	1	73259	73259	62.71	0.000
insulation method	1	5648166	5648166	4835.07	0.000
Square	3	23449	7816	6.69	0.001
HTC*HTC	1	323	323	0.28	0.601
Atm. Temperature(oC) * Atm.	1	170	170	0.15	0.704
Temperature(oC)					
Tip Temperature*Tip Temperature	1	22359	22359	19.14	0.000
2-Way Interaction	10	288947	28895	24.74	0.000
HTC*Atm. Temperature(oC)	1	0	0	0.00	0.999
HTC*Tip Temperature	1	2	2	0.00	0.969
HTC*chamber size	1	478	478	0.41	0.525
HTC*insulation method	1	1242	1242	1.06	0.307
Atm. Temperature(oC)*Tip Temperature	1	35	35	0.03	0.863
Atm. Temperature(oC)*chamber size	1	18	18	0.02	0.903
Atm. Temperature(oC)*insulation method	1	41	41	0.03	0.852
Tip Temperature*chamber size	1	55068	55068	47.14	0.000
Tip Temperature*insulation method	1	228425	228425	195.54	0.000
chamber size*insulation method	1	3638	3638	3.11	0.083
Error	61	71258	1168		
Lack-of-Fit	41	71258	1738	*	*
Pure Error	20	0	0		
Total	79	6116149			

Table 4.1: Findings from ANOVA for Von Mises stress.

					P-
Source	DF	Adj SS	Adj MS	F-Value	Value
Model	18	0.000754	0.000042	321.53	0.000
Linear	5	0.000700	0.000140	1075.01	0.000
НТС	1	0.000004	0.000004	28.06	0.000
Atm. Temperature(oC)	1	0.000000	0.000000	1.45	0.232
Tip Temperature	1	0.000037	0.000037	285.91	0.000
chamber size	1	0.000238	0.000238	1828.33	0.000
insulation method	1	0.000421	0.000421	3231.29	0.000
Square	3	0.000006	0.000002	15.29	0.000
HTC*HTC	1	0.000000	0.000000	1.08	0.303
Atm. Temperature(oC)*Atm.	1	0.000000	0.000000	0.43	0.515
Temperature(oC)					
Tip Temperature*Tip Temperature	1	0.000006	0.000006	42.97	0.000
2-Way Interaction	10	0.000048	0.000005	36.67	0.000
HTC*Atm. Temperature(oC)	1	0.000000	0.000000	0.00	0.996
HTC*Tip Temperature	1	0.000000	0.000000	0.16	0.693
HTC*chamber size	1	0.000000	0.000000	0.05	0.830
HTC*insulation method	1	0.000002	0.000002	18.40	0.000
Atm. Temperature(oC)*Tip Temperature	1	0.000000	0.000000	0.88	0.351
Atm. Temperature(oC)*chamber size	1	0.000000	0.000000	0.49	0.487
Atm. Temperature(oC)*insulation method	1	0.000000	0.000000	0.71	0.404
Tip Temperature*chamber size	1	0.000001	0.000001	10.35	0.002
Tip Temperature*insulation method	1	0.000018	0.000018	136.20	0.000
chamber size*insulation method	1	0.000026	0.000026	199.44	0.000
Error	61	0.000008	0.000000		
Lack-of-Fit	41	0.000008	0.000000	*	*
Pure Error	20	0.000000	0.000000		
Total	79	0.000762			

Table 4.2 : Findings from ANOVA for maximum deformation.

The pareto chart in Figure 4.14 below visually represents the magnitude and relative importance of each term in the regression model.

In both models, the Insulation method (E) emerges as the most significant factor. For the maximum stress model (Figure 4.14a), the interaction between the tip temperature and insulation method exists to be second most influential factor, followed by chamber size and tip temperature.

For the maximum deformation model (Figure 4.14b), chamber size exhibits the second most influential factor, followed by tip temperature and the interaction between chamber size and insulation method.

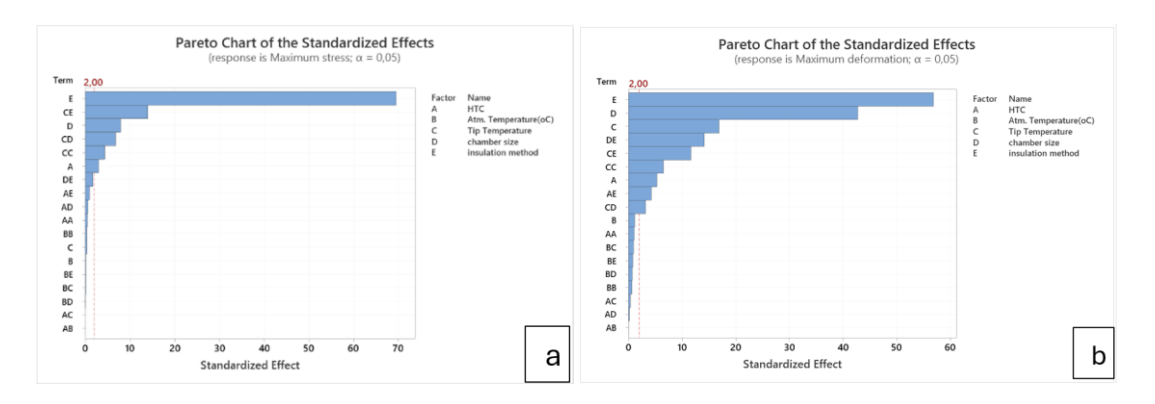


Figure 4.14: Pareto chart a) maximum stress, b) maximum deformation models.

Overall, the Pareto chart confirms that the structural behavior of the designed tool is highly affected by insulation mechanisms, chamber size, and cooling efficiency.

4.2.2. Response surface and interaction plots

To further understand the influence of input factors and their combined effects on the structural response of the tool, response surface plots and contour interaction plots were generated for both maximum stress and maximum deformation.

As indicated in Figure 4.15 below, the visualizations complement the statistical findings from the ANOVA by providing how the interactions of the input factors influence the maximum deformation.

The interaction between the tip temperature and atmospheric temperature shows the minimum effect on the deformation value, as indicated in Figure 4.15a and b, the maximum deformation of the tool slightly decreases with an increasing Heat transfer coefficient, while the atmospheric temperature has an insignificant effect on the maximum deformation value, as indicated by the near vertical contour bands along the atmospheric temperature axis. Figure 4.15c and d present the effect of the interaction

between the heat transfer coefficient and tip temperature. The result suggests that very high HTC leads to higher deformation, likely due to a steep thermal gradient. The result shows a non-linear interaction, and maximum deformation starts decreasing as the tip temperature increases. In Figure 4.15e and f, the interaction between tip temperature and atmospheric temperature is indicated, which visualizes decreasing maximum deformation with increasing value of tip temperature, which appears counterintuitive compared to typical thermal behaviour. This reflects that the applied boundary conditions reduce the thermal gradient and thereby limit overall deformation.

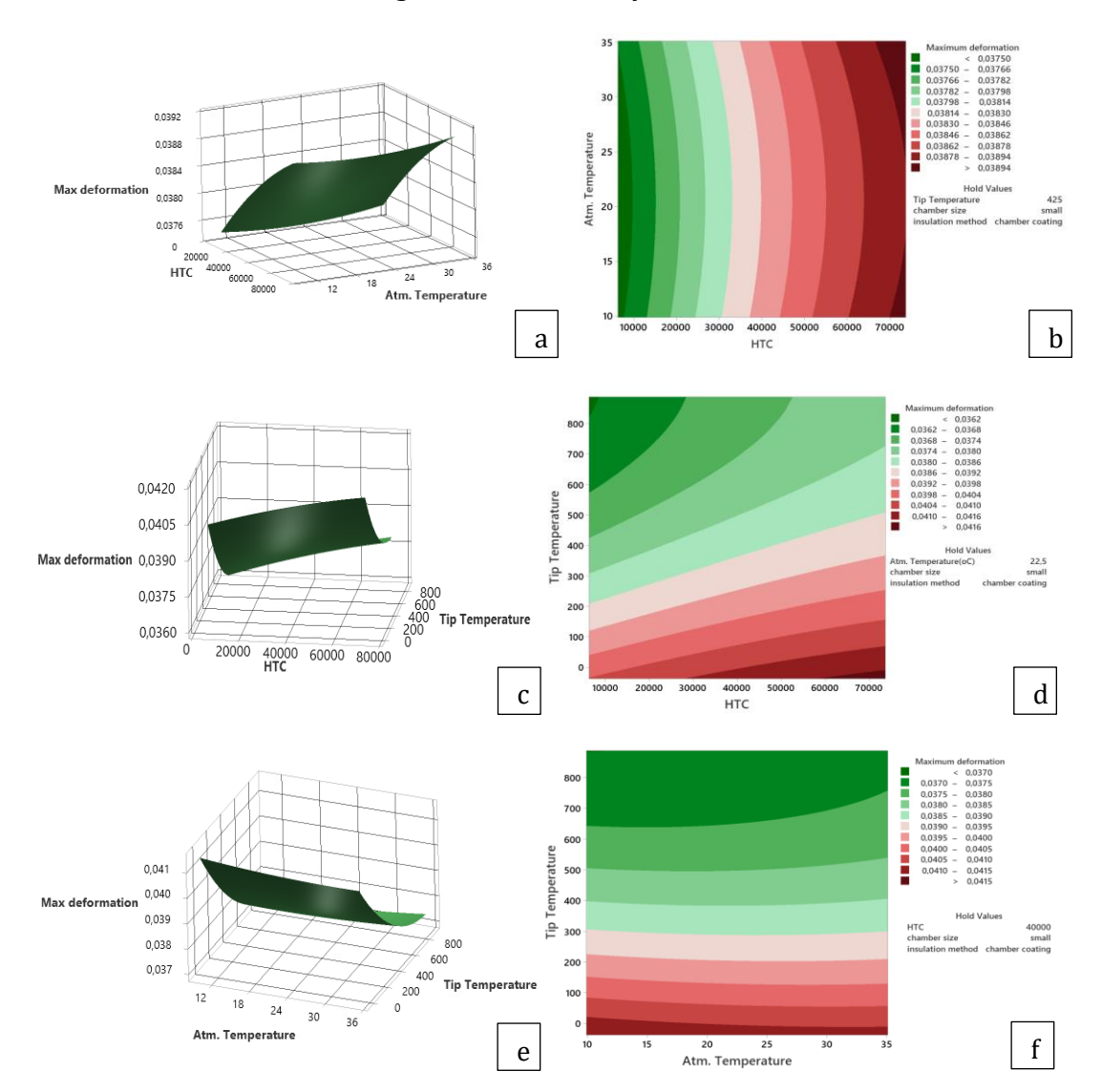


Figure 4.15: Response surface and interaction plots for maximum deformation of variant model 1.

Similarly, the effect of the key parameters on the maximum stress is illustrated in Figure 4.16. The combination of the Heat transfer coefficient and atmospheric temperature (Figure 4.16a and b) demonstrates that maximum stress throughout the tool increases

with increasing HTC due to the increased thermal gradients, and the effect of atmospheric temperature is negligible, as indicated by almost vertical contour bands.

The interaction of HTC and tip temperature (Figure 4.16c and d) clearly show that maximum stress is higher at high tip temperature and HTC due to the development of large thermal gradients and constrained thermal expansion. A high HTC value rapidly extracts heat from the tool tip, which creates a sharp thermal gradient across the tool structure and induces substantial thermal stress. Therefore, high von Mises stress is introduced during the combination of high tip temperature with high heat transfer coefficient.

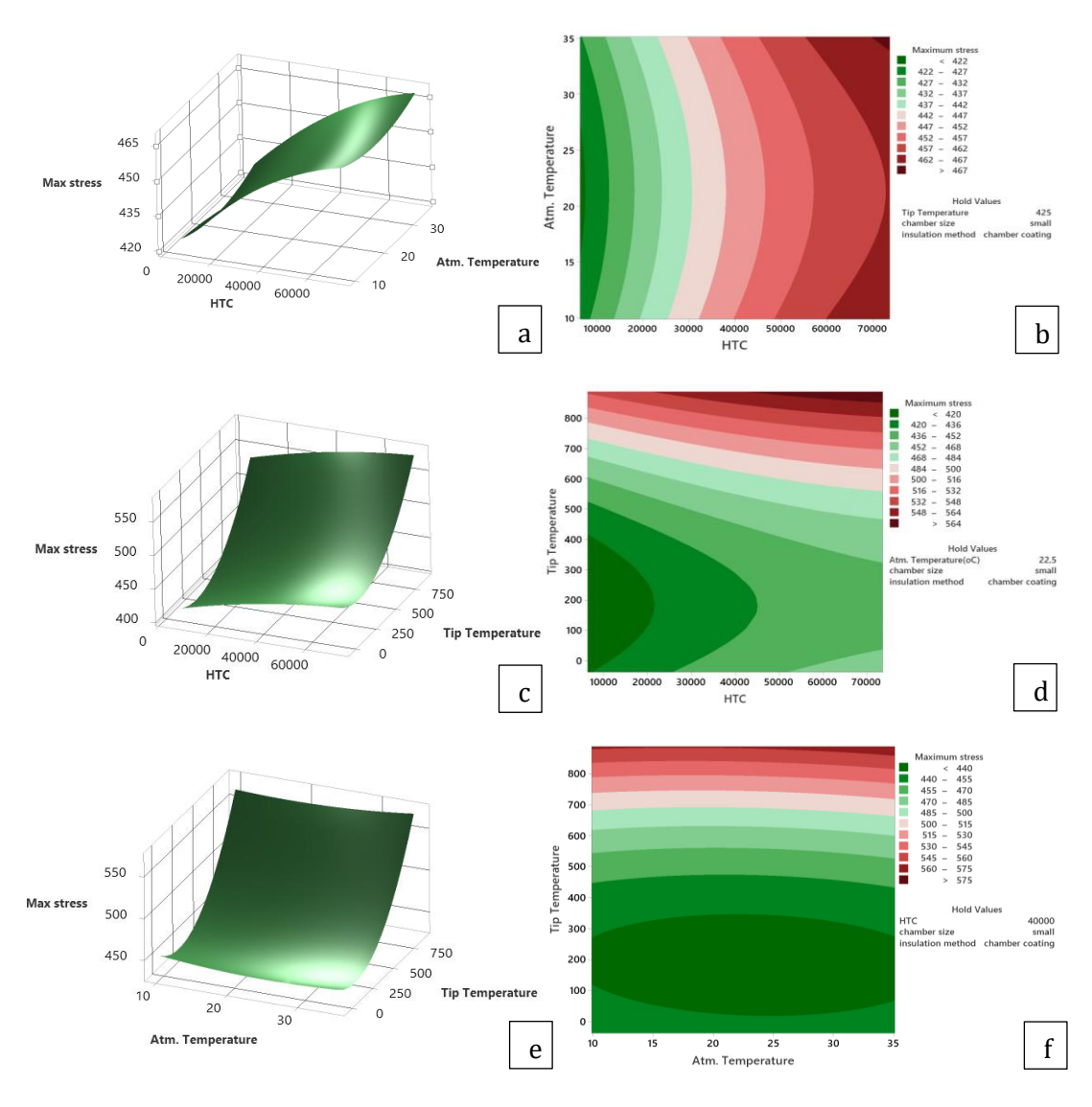


Figure 4.16 : Response surface and interaction plots for maximum stress of variant model 1.

The effects of the continuous and categorical factors are captured by using the regression equation for maximum stress and deformation derived using RSM, provided in Appendix C, enabling the prediction of responses within the design matrix and optimization without repeated simulations.

For the configuration with an insulation pad between the cutting tool head and shank, as shown in Figure 4.17 The effect of the parameters on maximum deformation. It is observed that, unlike the configuration with a chamber coating, which is presented in Figure 4.15c and d the maximum deformation throughout the tool increases at high tip temperature and low tip temperature, which is caused by the effect of the insulation method and thermal gradient in the tool.

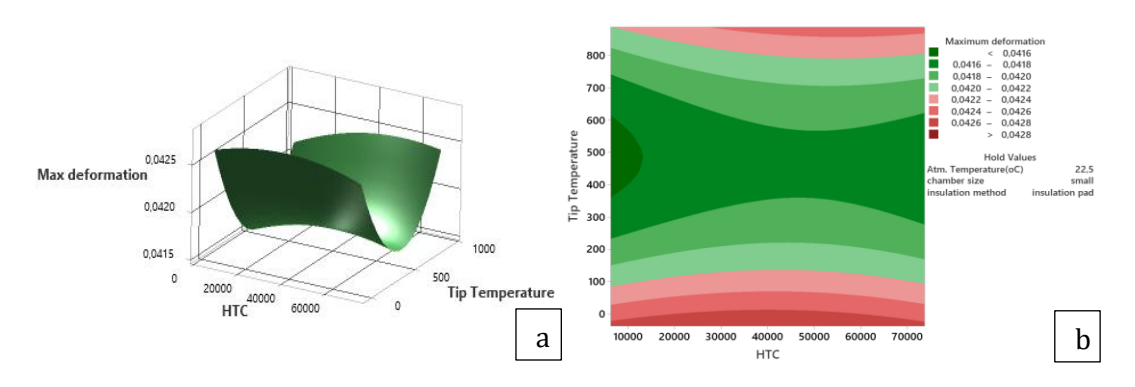


Figure 4.17 : Response surface and interaction plot for maximum deformation of variant model 2.

The effect of an insulation method on the maximum stress distribution observed is presented in Figure 4.18 which shows that the increased HTC at high tool tip temperature results in a slight increase in maximum Von Mises stress in the tool due to the increased temperature gradient. Also, it is observed that the maximum stress in the configuration with an insulation pad between the tool head and shank is at the combination of low tool tip temperature and high heat transfer coefficient of LN_2

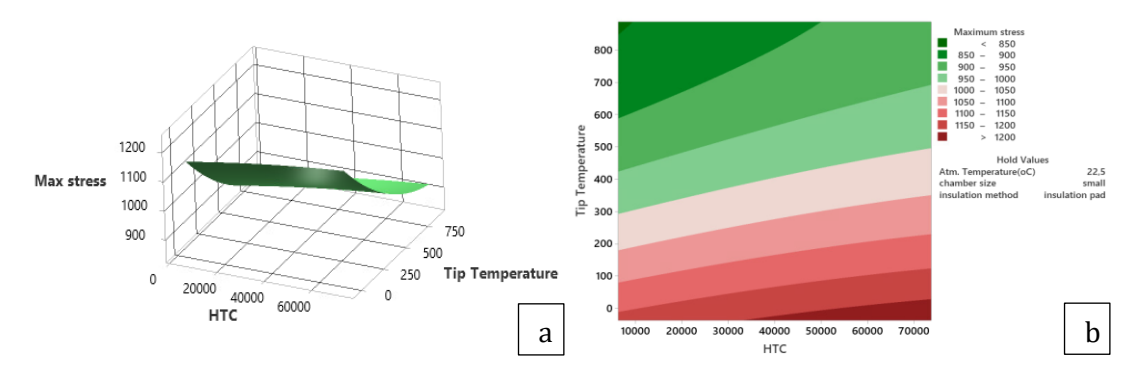


Figure 4.18 : Response surface and interaction plot for maximum stress of variant model 2.

Chapter 5

Conclusion and future work

5.1. Conclusion

The current research study focused on the development and evaluation of cryogenic cooling strategies for a turning tool with internal cooling via liquid nitrogen (LN_2). A comprehensive simulation-based methodology was employed to investigate the thermal and structural response of various design configurations under both dry and cryogenically cooled machining scenarios. The influence of the key parameters and their interactions on the maximum stress distribution and peak deformation throughout the tool was analysed using response surface methodology (RSM).

A total of 80 simulations were conducted based on a structured Design of Experiments (DOE) matrix. The temperature distribution under different cooling conditions was determined by conducting Steady-state thermal analyses, followed by structural analysis incorporating the thermal load from the steady-state thermal analysis and machining forces. Two key design configurations were studied in detail: one incorporating an insulation coating within the Liquid nitrogen chamber and another placing an insulation pad between the tool head and shank. The simulation results indicated that the localized cooling and reduced heat propagation due to the chamber-insulated configuration provided superior thermal performance and lower thermal stress and deformation.

The structural analysis revealed that the maximum von Mises stress was concentrated near the cutting tip, but it was also significantly high at the head-shank interface. The cryogenic setup with chamber coating reduced the maximum stress by more than 60% compared to the dry case and by 59.5% compared to the cryogenic setup under the configuration with an insulation pad between the tool head and shank. Proof of strength evaluations confirmed that the design remained structurally safe under all simulated conditions, with values above 1 even in the worst-case scenario and 2.93 for the configuration with liquid nitrogen chamber coating.

Furthermore, different tool head materials were evaluated, and it was found that material selection had a negligible effect on maximum stress due to the dominant influence of thermal gradients, but tool steel H13 stands out as the tool head material based on its manufacturability, high strength, toughness, and all other properties. From a thermal point of view, however, the alloy Ti-6Al-4V is attractive due to the low thermal conductivity providing a temperature-dependent insulation effect, which is beneficial for the delivery system connected with the expansion chamber [66].

Parametric analysis using RSM and ANOVA revealed that the insulation method was the most influential parameter for the tool design. heat transfer coefficient (HTC), tip temperature, and chamber size were also parameters with significant influence affecting stress and deformation. Interaction plots and response surfaces provided valuable insights into the nonlinear behavior and complex interdependencies between these factors.

In conclusion, the integration of LN_2 cooling with strategically placed insulation demonstrates strong potential for improving tool holder reliability and performance in high-temperature machining applications. This approach effectively minimizes thermal loading, reduces deformation, and enhances structural stability. The findings offer a promising design guideline for cryogenic tool holder systems.

Key Findings:

- A tool with an integrated chamber for liquid nitrogen cooling is successfully designed.
- The tool design with ${\rm LN_2}$ chamber insulation achieved the lowest thermal stress and deformation.
- Dry machining conditions resulted in significantly higher stress levels, particularly near the tool tip and at the head-shank interface.
- Cryogenic cooling with chamber coating reduced the maximum Von Mises stress by over 63% compared to dry conditions and 59.5% compared to the configuration with an insulation pad between the tool head and shank.
- The factor of safety remained above 1 across all configurations, ensuring structural integrity with the maximum value of 2.93 for the configuration with insulation coating of the liquid nitrogen chamber.
- Material selection for the tool head showed minimal influence on the stress response under the applied loads.

- RSM and ANOVA confirmed that HTC, tip temperature, insulation method, and chamber size were the most influential parameters.
- Interaction plots highlighted complex interdependencies between thermal and geometric variables.

5.2. Future work

While the current study offers valuable insights, several aspects remain open for further research. First, experimental validation of the simulation results would be essential to enhance and confirm the accuracy of the simulation and ensure the practical applicability of the proposed design. Additionally, extending the current work using CFD thermal simulations, including thermal phase change and pressure-based phase change, and fatigue life analysis, could provide a more comprehensive understanding of the tool holder's long-term behaviour, with a deeper understanding of the cooling dynamics during machining. Future studies could also explore optimization of internal chamber geometry for LN_2 flow, additive manufacturing possibilities for integrated cooling structures, and the combined effect of tool wear and thermal cycling in real cutting environments. Generally, the major focus for the future is to develop a hybrid cooling approach with superior HTC, without the side effects of massive undercooling of the whole tool structure and linked performance loss.

Appendix A

Design of experiment detailed table

Run	Pt			Atm.	Tip				Max.
Orde	Тур	Blo	LN ₂	Tem	Temp	chamb	insulatio	Max.	Deformati
r	е	cks	HTC	(°C)	(°C)	er size	n method	stress	on
			2000				chamber	451.3	
1	1	1	0	15	150	small	coating	3	0.03943
			6000				chamber	502.5	
12	1	1	0	15	150	small	coating	4	0.040054
			2000				chamber		
3	1	1	0	30	150	small	coating	451	0.039398
			6000				chamber	502.2	
4	1	1	0	30	150	small	coating	9	0.040021
			2000				chamber		
5	1	1	0	15	700	small	coating	509.4	0.037277
			6000				chamber	528.9	
6	1	1	0	15	700	small	coating	8	0.037988
			2000				chamber	509.3	
7	1	1	0	30	700	small	coating	4	0.037277
			6000				chamber	528.9	
8	1	1	0	30	700	small	coating	3	0.037979
			6364				chamber	387.0	
9	-1	1	.143	22.5	425	small	coating	9	0.036972
			7363				chamber	415.1	
10	-1	1	5.86	22.5	425	small	coating	9	0.038621
			4000				chamber	408.5	
11	-1	1	0	9.887	425	small	coating	3	0.038199
			4000				chamber	408.4	
12	-1	1	0	35.11	425	small	coating	4	0.038164
			4000		-		chamber	570.0	
13	-1	1	0	22.5	37.493	small	coating	4	0.041714
			4000		887.49		chamber	600.7	
14	-1	1	0	22.5	3	small	coating	9	0.037949
			4000				chamber	408.4	
15	0	1	0	22.5	425	small	coating	8	0.038181
			4000				chamber	408.4	
16	0	1	0	22.5	425	small	coating	8	0.038181
			4000				chamber	408.4	
17	0	1	0	22.5	425	small	coating	8	0.038181
			4000				chamber	408.4	
18	0	1	0	22.5	425	small	coating	8	0.038181

			4000				chamber	408.4	
19	0	1	4000	22.5	425	small	coating	406.4 8	0.038181
19	U		4000	22.3	423	Siliali	chamber	408.4	0.038181
20	0	1	0	22.5	425	small	coating	8	0.038181
20	- 0		2000	22.3	423	Siliali	chamber	288.3	0.036161
21	1	1	0	15	150	big	coating	200.3	0.042428
21			6000	13	130	Dig	chamber	293.0	0.042428
22	1	1	0	15	150	big	coating	293.0	0.042919
22	-		2000	13	130	Dig	chamber	288.2	0.042313
23	1	1	0	30	150	big	coating	7	0.042388
23			6000	30	130	DIB	chamber	292.9	0.042300
24	1	1	0	30	150	big	coating	7	0.042879
	_		2000			7.8	chamber	527.7	0.0.120.0
25	1	1	0	15	700	big	coating	1	0.038496
	_		6000			~.8	chamber	540.3	0.000.00
26	1	1	0	15	700	big	coating	9	0.040101
	_		2000			~.8	chamber	527.6	0.0.0202
27	1	1	0	30	700	big	coating	6	0.038443
	_		6000			~.8	chamber	540.3	0.0001.0
28	1	1	0	30	700	big	coating	5	0.040045
	_	_	6364			3.8	chamber	397.4	0.0.00.0
29	-1	1	.143	22.5	425	big	coating	5	0.039286
	_	_	7363			3.8	chamber	416.1	0.000200
30	-1	1	5.86	22.5	425	big	coating	6	0.041168
	_		4000			~.8	chamber	411.9	0.0.1220
31	-1	1	0	9.887	425	big	coating	2	0.040604
			4000			- 0	chamber	411.8	
32	-1	1	0	35.11	425	big	coating	5	0.040506
			4000		-		chamber	254.9	
33	-1	1	0	22.5	37.493	big	coating	6	0.044818
			4000		887.49		chamber	621.7	
34	-1	1	0	22.5	3	big	coating	1	0.038944
			4000				chamber	411.8	
35	0	1	0	22.5	425	big	coating	9	0.040555
			4000				chamber	411.8	
36	0	1	0	22.5	425	big	coating	9	0.040555
			4000				chamber	411.8	
37	0	1	0	22.5	425	big	coating	9	0.040555
			4000				chamber	411.8	
38	0	1	0	22.5	425	big	coating	9	0.040555
			4000				chamber	411.8	
39	0	1	0	22.5	425	big	coating	9	0.040555
			4000				chamber	411.8	
40	0	1	0	22.5	425	big	coating	9	0.040555
			2000				insulation	1068.	
41	1	1	0	15	150	small	pad	5	0.042184
			6000				insulation	1096.	
42	1	1	0	15	150	small	pad	3	0.04234
			2000				insulation	1067.	
43	1	1	0	30	150	small	pad	3	0.042106

			6000				insulation	1095.	
44	1	1	0	30	150	small	pad	1093.	0.042263
44			2000	30	130	Siliali	insulation	904.0	0.042203
45	1	1	0	15	700	small	pad	904.0 1	0.041636
43			6000	13	700	Siliali	insulation	_	0.041030
46	1	1	0	15	700	small	pad	8	0.041847
40			2000	13	700	Siliali	insulation	902.7	0.041847
47	1	1	0	30	700	small	pad	6	0.041554
47	-		6000	30	700	Siliali	insulation	951.8	0.041334
48	1	1	0	30	700	small	pad	9	0.041766
70			6364	30	700	Jillali	insulation	957.6	0.041700
49	-1	1	.143	22.5	425	small	pad	8	0.041689
1.5			7363	22.5	123	Sirian	insulation	1031.	0.011003
50	-1	1	5.86	22.5	425	small	pad	1	0.042051
30			4000	22.0	123	Simun	insulation	1010.	0.0 .2031
51	-1	1	0	9.887	425	small	pad	6	0.042009
	_		4000	0.007		0111011	insulation	1008.	0.0.12000
52	-1	1	0	35.11	425	small	pad	5	0.041875
	_		4000		-	0111011	insulation	1136.	0.0.120.0
53	-1	1	0	22.5	37.493	small	pad	7	0.042494
	_		4000		887.49	0111011	insulation	882.4	0.0.12.0.1
54	-1	1	0	22.5	3	small	pad	2	0.041626
	_	_	4000			0111011	insulation	1009.	0.0.12020
55	0	1	0	22.5	425	small	pad	5	0.041942
			4000				insulation	1009.	
56	0	1	0	22.5	425	small	pad	5	0.041942
			4000				insulation	1009.	
57	0	1	0	22.5	425	small	pad	5	0.041942
			4000				insulation	1009.	
58	0	1	0	22.5	425	small	pad	5	0.041942
			4000				insulation	1009.	
59	0	1	0	22.5	425	small	pad	5	0.041942
			4000				insulation	1009.	
60	0	1	0	22.5	425	small	pad	5	0.041942
			2000				insulation	982.1	
61	1	1	0	15	150	big	pad	9	0.04748
			6000				insulation	1007.	
62	1	1	0	15	150	big	pad	4	0.047682
			2000				insulation	964.6	
63	1	1	0	30	150	big	pad	8	0.046488
			6000				insulation	989.8	
64	1	1	0	30	150	big	pad	8	0.04669
			2000				insulation	870.1	
65	1	1	0	15	700	big	pad	6	0.046917
			6000				insulation	901.4	
66	1	1	0	15	700	big	pad	5	0.046274
			2000				insulation		
67	1	1	0	30	700	big	pad	869.1	0.046875
			6000				insulation	900.4	
68	1	1	0	30	700	big	pad	5	0.046232

			6364				insulation	877.0	
69	-1	1	.143	22.5	425	big	pad	1	0.045976
			7363				insulation	951.5	
70	-1	1	5.86	22.5	425	big	pad	1	0.0465
			4000				insulation	933.7	
71	-1	1	0	9.887	425	big	pad	5	0.046399
			4000				insulation	932.0	
72	-1	1	0	35.11	425	big	pad	3	0.046328
			4000		-		insulation	1014.	
73	-1	1	0	22.5	37.493	big	pad	6	0.046858
			4000		887.49		insulation	851.1	
74	-1	1	0	22.5	3	big	pad	9	0.046028
			4000				insulation	932.8	
75	0	1	0	22.5	425	big	pad	9	0.046364
			4000				insulation	932.8	
76	0	1	0	22.5	425	big	pad	9	0.046364
			4000				insulation	932.8	
77	0	1	0	22.5	425	big	pad	9	0.046364
			4000				insulation	932.8	
78	0	1	0	22.5	425	big	pad	9	0.046364
			4000				insulation	932.8	
79	0	1	0	22.5	425	big	pad	9	0.046364
			4000				insulation	932.8	
80	0	1	0	22.5	425	big	pad	9	0.046364

Table A. 1: DOE matrix table with simulation results of maximum stress and maximum deformation.

Appendix B

Residual analysis plots

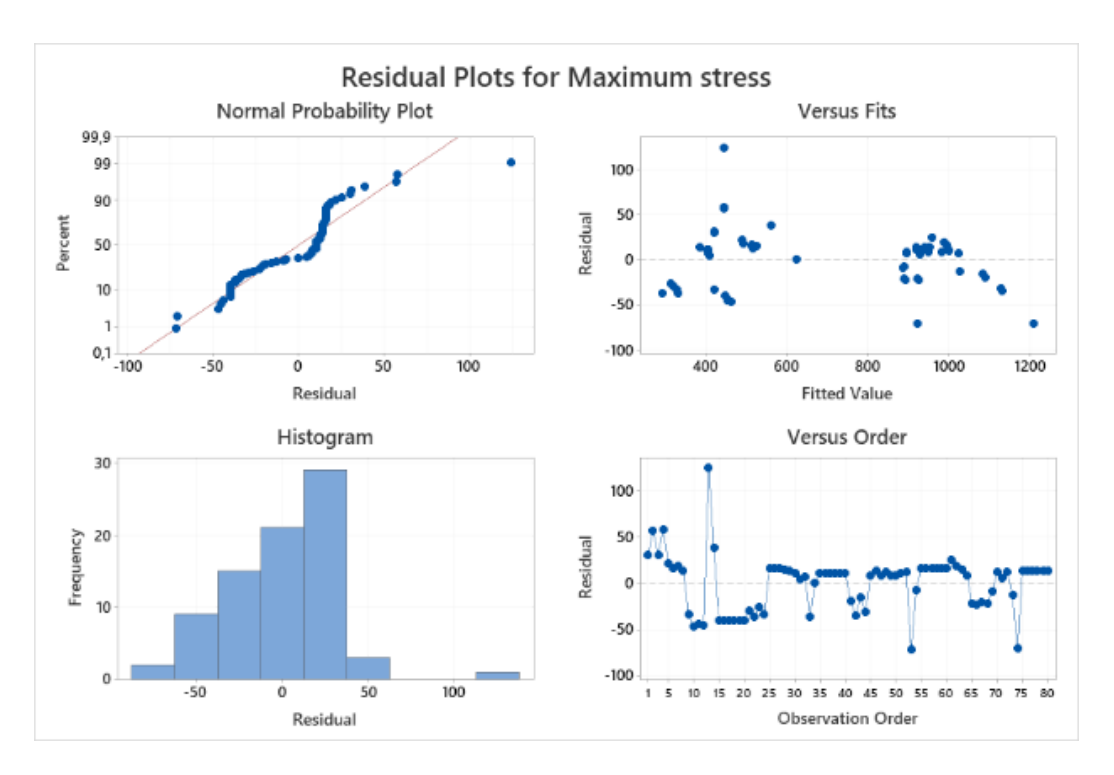


Figure B. 1: Residual Plots for maximum stress

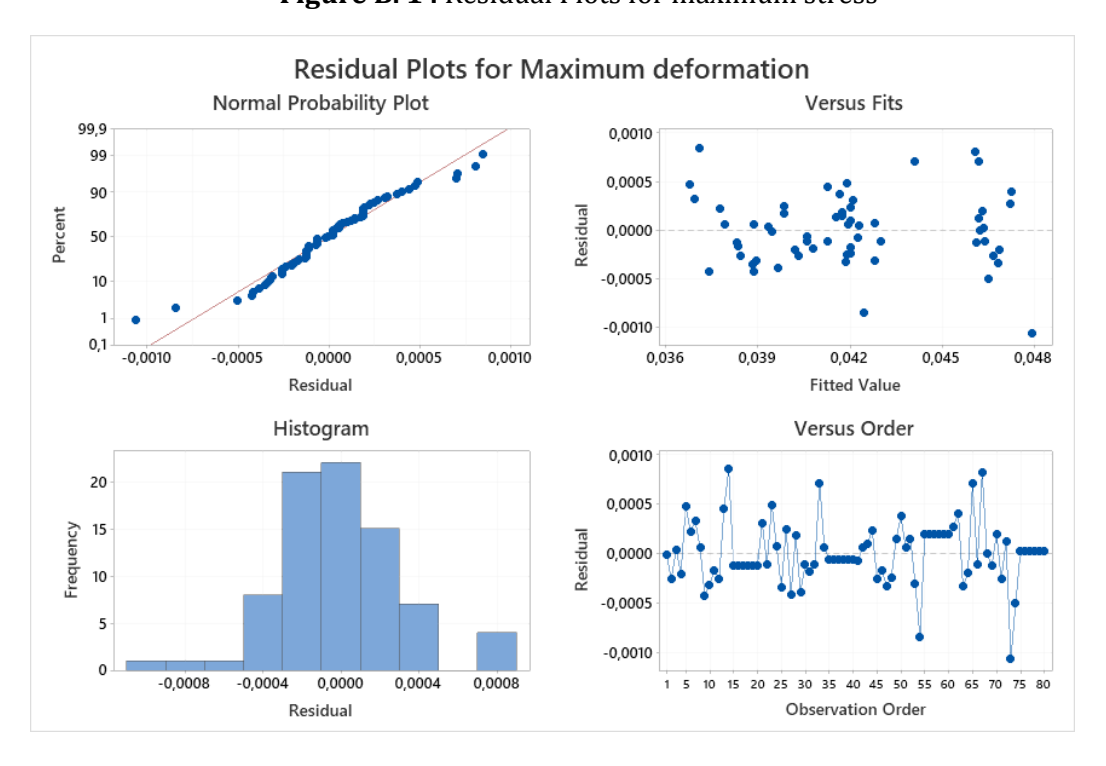


Figure B. 2: Residual plots for maximum deformation

Appendix C

Regression equations for the models

Regression Equation in Uncoded Units

small	chamber coating	Maximum stress = 427,2 + 0,00107 HTC
		- 1,52 Atm. Temperature(oC)- 0,1087 Tip Temperature - 0,000000 HTC*HTC+ 0,0305 Atm. Temperature(oC)*Atm. Temperature(oC)
		ure(oC) + 0,000260 Tip Temperature*Tip Temperature + 0,000000 HTC*Atm. Temperature(oC) + 0,000000 HTC*Tip Temperature + 0,00051 Atm. Temperature(oC)*Tip Temperature
big	chamber coating	Maximum stress = 297,3 + 0,00077 HTC
Jig	chamber couching	- 1,67 Atm. Temperature(oC) + 0,1222 Tip Temperature - 0,000000 HTC*HTC + 0,0305 Atm. Temperature(oC)*Atm. Temperature(oC) + 0,000260 Tip Temperature*Tip Temperature + 0,000000 HTC*Atm. Temperature(oC) + 0,000000 HTC*Tip Temperature + 0,00051 Atm. Temperature(oC)*Tip Temperature
small	insulation pad	Maximum stress = 1158,1 + 0,00155 HTC - 1,75 Atm. Temperature(oC) - 0,5790 Tip Temperature - 0,000000 HTC*HTC + 0,0305 Atm. Temperature(oC)*Atm. Temperature(oC) + 0,000260 Tip Temperature*Tip Temperature + 0,000000 HTC*Atm. Temperature(oC) + 0,000000 HTC*Tip Temperature + 0,00051 Atm. Temperature(oC)*Tip Temperature
big	insulation pad	Maximum stress = 1001,2 + 0,00125 HTC - 1,90 Atm. Temperature(oC) - 0,3481 Tip Temperature - 0,000000 HTC*HTC + 0,0305 Atm. Temperature(oC)*Atm. Temperature(oC) + 0,000260 Tip Temperature*Tip Temperature + 0,000000 HTC*Atm. Temperature(oC) + 0,000000 HTC*Tip Temperature + 0,00051 Atm. Temperature(oC)*Tip Temperature

Figure C. 1: Regression equations for maximum stress

Regression Equation in Uncoded Units

small	size insulation metho chamber coating		= 0,040437 + 0,000000 HTC - 0,000035 Atm. Temperature(oC) - 0,000009 Tip Temperature - 0,000000 HTC*HTC + 0,000001 Atm. Temperature(oC)*Atm. Temperature(oC) + 0,000000 Tip Temperature*Tip Temperature - 0,000000 HTC*Atm. Temperature(oC) + 0,000000 HTC*Tip Temperature - 0,000000 Atm. Temperature(oC)*Tip Temperature
big	chamber coating	Maximum deformation :	= 0,043397 + 0,000000 HTC - 0,000044 Atm. Temperature(oC) - 0,000010 Tip Temperature - 0,000000 HTC*HTC + 0,000001 Atm. Temperature(oC)*Atm. Temperature(oC) + 0,000000 Tip Temperature*Tip Temperature - 0,000000 HTC*Atm. Temperature(oC) + 0,000000 HTC*Tip Temperature + 0,000000 Atm. Temperature(oC)*Tip Temperature
small	insulation pad	Maximum deformation :	= 0,043208 + 0,000000 HTC - 0,000046 Atm. Temperature(oC) - 0,000005 Tip Temperature - 0,000000 HTC*HTC + 0,000001 Atm. Temperature(oC)*Atm. Temperature(oC) + 0,000000 Tip Temperature*Tip Temperature - 0,000000 HTC*Atm. Temperature(oC) + 0,000000 HTC*Tip Temperature + 0,000000 Atm. Temperature(oC)*Tip Temperature
big	insulation pad	Maximum deformation :	= 0,048448 + 0,000000 HTC - 0,000055 Atm. Temperature(oC) - 0,000006 Tip Temperature - 0,000000 HTC*HTC + 0,000001 Atm. Temperature(oC)*Atm. Temperature(oC) + 0,000000 Tip Temperature*Tip Temperature - 0,000000 HTC*Atm. Temperature(oC) + 0,000000 HTC*Tip Temperature - 0,000000 Atm. Temperature(oC)*Tip Temperature

Figure C. 2: Regression equations for maximum deformation

Bibliography

- [1] Shane. Y. Hong, "US patent," 1999.
- [2] N. A. Abukhshim, P. T. Mativenga, and M. A. Sheikh, "Heat generation and temperature prediction in metal cutting: A review and implications for high speed machining," *Int J Mach Tools Manuf*, vol. 46, no. 7–8, pp. 782–800, Jun. 2006, doi: 10.1016/j.ijmachtools.2005.07.024.
- [3] G. Hao and Z. Liu, "The heat partition into cutting tool at tool-chip contact interface during cutting process: a review," *International Journal of Advanced Manufacturing Technology*, vol. 108, no. 1–2, pp. 393–411, May 2020, doi: 10.1007/s00170-020-05404-9.
- [4] B. Jerry p., "Metalworking Fluids Second Edition," 2006.
- [5] M. A. E. Baradie, "Materials Processing Technology CUTTING FLUIDS: PART I. CHARACTERISATION," 1996.
- [6] M. C. Shaw, "ON THE ACTION OF METAL CUTTING FLUIDS AT LOW SPEEDS*."
- [7] I. S. Jawahir *et al.*, "Cryogenic manufacturing processes," *CIRP Ann Manuf Technol*, vol. 65, no. 2, pp. 713–736, 2016, doi: 10.1016/j.cirp.2016.06.007.
- [8] B. Boswell, M. N. Islam, I. J. Davies, Y. R. Ginting, and A. K. Ong, "A review identifying the effectiveness of minimum quantity lubrication (MQL) during conventional machining," *International Journal of Advanced Manufacturing Technology*, vol. 92, no. 1–4, pp. 321–340, Sep. 2017, doi: 10.1007/s00170-017-0142-3.
- [9] A. B. Chattopadhyay, A. Bose, and A. K. Chattopdhyay, "Improvements in grinding steels by cryogenic cooling."
- [10] W. S. Hollis, "THE APPLICATION AND EFFECT OF CONTROLLED ATMOSPHERES IN THE MACHINING OF METALS," Pergamon Press, 1961.
- [11] N. Khanna *et al.*, "Review on design and development of cryogenic machining setups for heat resistant alloys and composites," Aug. 01, 2021, *Elsevier Ltd.* doi: 10.1016/j.jmapro.2021.05.053.
- [12] Y. Yildiz and M. Nalbant, "A review of cryogenic cooling in machining processes," Jul. 2008. doi: 10.1016/j.ijmachtools.2008.01.008.

- [13] A. Bagherzadeh and E. Budak, "Investigation of machinability in turning of difficult-to-cut materials using a new cryogenic cooling approach," *Tribol Int*, vol. 119, pp. 510–520, Mar. 2018, doi: 10.1016/j.triboint.2017.11.033.
- [14] T. C. Yap, "Roles of Cryogenic Cooling in Turning of Superalloys, Ferrous Metals, and Viscoelastic Polymers," Sep. 01, 2019, MDPI. doi: 10.3390/technologies7030063.
- [15] Chetan, S. Ghosh, and P. V. Rao, "Comparison between sustainable cryogenic techniques and nano-MQL cooling mode in turning of nickel-based alloy," *J Clean Prod*, vol. 231, pp. 1036–1049, Sep. 2019, doi: 10.1016/j.jclepro.2019.05.196.
- [16] C. Courbon, F. Pusavec, F. Dumont, J. Rech, and J. Kopac, "Influence of cryogenic lubrication on the tribological properties of Ti6Al4V and Inconel 718 alloys under extreme contact conditions," in *Lubrication Science*, John Wiley and Sons Ltd, 2014, pp. 315–326. doi: 10.1002/ls.1254.
- [17] Pusavec F, "porous tungsten cryogenic cooling," *Int J Refract Metals Hard Mater*, 2012.
- [18] F. Pusavec *et al.*, "Analysis of the influence of nitrogen phase and surface heat transfer coefficient on cryogenic machining performance," *J Mater Process Technol*, vol. 233, pp. 19–28, Jul. 2016, doi: 10.1016/j.jmatprotec.2016.02.003.
- [19] B. Dilip Jerold and M. Pradeep Kumar, "Experimental comparison of carbon-dioxide and liquid nitrogen cryogenic coolants in turning of AISI 1045 steel," *Cryogenics (Guildf)*, vol. 52, no. 10, pp. 569–574, Oct. 2012, doi: 10.1016/j.cryogenics.2012.07.009.
- [20] A. Saeed, "Joule Thomson Effect," 2022.
- [21] A. Bagherzadeh and E. Budak, "Investigation of machinability in turning of difficult-to-cut materials using a new cryogenic cooling approach," *Tribol Int*, vol. 119, pp. 510–520, Mar. 2018, doi: 10.1016/j.triboint.2017.11.033.
- [22] F. Pusavec *et al.*, "Analysis of the influence of nitrogen phase and surface heat transfer coefficient on cryogenic machining performance," *J Mater Process Technol*, vol. 233, pp. 19–28, Jul. 2016, doi: 10.1016/j.jmatprotec.2016.02.003.
- [23] M. Hribersek, V. Sajn, F. Pusavec, J. Rech, and J. Kopac, "The Procedure of Solving the Inverse Problem for Determining Surface Heat Transfer Coefficient between Liquefied Nitrogen and Inconel 718 Workpiece in Cryogenic Machining," in

- *Procedia CIRP*, Elsevier B.V., 2017, pp. 617–622. doi: 10.1016/j.procir.2017.03.227.
- [24] Y. Wang, M. Dai, K. Liu, J. Liu, L. Han, and H. Liu, "Research on surface heat transfer mechanism of liquid nitrogen jet cooling in cryogenic machining," *Appl Therm Eng*, vol. 179, Oct. 2020, doi: 10.1016/j.applthermaleng.2020.115607.
- [25] S. Y. Hong and Y. Ding, "Micro-temperature manipulation in cryogenic machining of low carbon steel," 2001.
- [26] M. Dix, R. Wertheim, G. Schmidt, and C. Hochmuth, "Modeling of drilling assisted by cryogenic cooling for higher efficiency," *CIRP Ann Manuf Technol*, vol. 63, no. 1, pp. 73–76, 2014, doi: 10.1016/j.cirp.2014.03.080.
- [27] G. Rotella and D. Umbrello, "Finite element modeling of microstructural changes in dry and cryogenic cutting of Ti6Al4V alloy," *CIRP Ann Manuf Technol*, vol. 63, no. 1, pp. 69–72, 2014, doi: 10.1016/j.cirp.2014.03.074.
- [28] M. F. Novella, S. Sartori, M. Bellin, A. Ghiotti, and S. Bruschi, "Modelling the Thermo-mechanical Behavior of a Redesigned Tool Holder to Reduce the Component Geometrical Deviations in Cryogenic Machining," in *Procedia CIRP*, Elsevier B.V., 2017, pp. 347–352. doi: 10.1016/j.procir.2017.03.236.
- [29] A. H. Kheireddine, A. H. Ammouri, T. Lu, O. W. Dillon, R. F. Hamade, and I. S. Jawahir, "An experimental and numerical study of the effect of cryogenic cooling on the surface integrity of drilled holes in AZ31B Mg alloy," *International Journal of Advanced Manufacturing Technology*, vol. 78, no. 1–4, pp. 269–279, Apr. 2015, doi: 10.1007/s00170-014-6650-5.
- [30] S. Y. Hong and Y. Ding, "Cooling approaches and cutting temperatures in cryogenic machining of Ti-6Al-4V," 2001.
- [31] D. Umbrello, F. Micari, and I. S. Jawahir, "The effects of cryogenic cooling on surface integrity in hard machining: A comparison with dry machining," *CIRP Ann Manuf Technol*, vol. 61, no. 1, pp. 103–106, 2012, doi: 10.1016/j.cirp.2012.03.052.
- [32] D. Biermann and H. Hartmann, "Reduction of burr formation in drilling using cryogenic process cooling," in *Procedia CIRP*, Elsevier B.V., 2012, pp. 85–90. doi: 10.1016/j.procir.2012.07.016.
- [33] M. J. Bermingham, J. Kirsch, S. Sun, S. Palanisamy, and M. S. Dargusch, "New observations on tool life, cutting forces and chip morphology in cryogenic

- machining Ti-6Al-4V," *Int J Mach Tools Manuf*, vol. 51, no. 6, pp. 500–511, Jun. 2011, doi: 10.1016/j.ijmachtools.2011.02.009.
- [34] S. Chaabani, P. J. Arrazola, Y. Ayed, A. Madariaga, A. Tidu, and G. Germain, "Comparison between cryogenic coolants effect on tool wear and surface integrity in finishing turning of Inconel 718," *J Mater Process Technol*, vol. 285, Nov. 2020, doi: 10.1016/j.jmatprotec.2020.116780.
- [35] M. Dhananchezian, M. Rishaba Priyan, G. Rajashekar, and S. S. Narayanan, "Study The Effect Of Cryogenic Cooling On Machinability Characteristics During Turning Duplex Stainless Steel 2205," 2018. [Online]. Available: www.sciencedirect.comwww.materialstoday.com/proceedings2214-7853
- [36] Z. Y. Wang, K. P. Rajurkar, J. Fan, S. Lei, Y. C. Shin, and G. Petrescu, "Hybrid machining of Inconel 718," *Int J Mach Tools Manuf*, vol. 43, no. 13, pp. 1391–1396, Oct. 2003, doi: 10.1016/S0890-6955(03)00134-2.
- [37] Z. Y. Wang, K. P. Rajurkar, and M. Murugappan, "Cryogenic PCBN turning of ceramic (S&N,)," 1996.
- [38] R. Peng, H. Jiang, X. Tang, X. Huang, Y. Xu, and Y. Hu, "Design and performance of an internal-cooling turning tool with micro-channel structures," *J Manuf Process*, vol. 45, pp. 690–701, Sep. 2019, doi: 10.1016/j.jmapro.2019.08.011.
- [39] T. Minton, S. Ghani, F. Sammler, R. Bateman, P. Fürstmann, and M. Roeder, "Temperature of internally-cooled diamond-coated tools for dry-cutting titanium," *Int J Mach Tools Manuf*, vol. 75, pp. 27–35, 2013, doi: 10.1016/j.ijmachtools.2013.08.006.
- [40] R. Y. Chiou, L. Lu, J. S. J. Chen, and M. T. North, "Investigation of dry machining with embedded heat pipe cooling by finite element analysis and experiments," *International Journal of Advanced Manufacturing Technology*, vol. 31, no. 9–10, pp. 905–914, Jan. 2007, doi: 10.1007/s00170-005-0266-8.
- [41] E. Uhlmann, J. Polte, J. Fasselt, C. Schmiedel, B. Hein, and N. Welteke, "Additive manufacturing of an internally cooled tool holder for turning," 2024. [Online]. Available: www.euspen.eu
- [42] P. Albertelli, V. Mussi, M. Strano, and M. Monno, "Experimental investigation of the effects of cryogenic cooling on tool life in Ti6Al4V milling", doi: 10.1007/s00170-021-07161-9/Published.

- [43] T. Lu, R. Kudaravalli, and G. Georgiou, "Cryogenic Machining through the Spindle and Tool for Improved Machining Process Performance and Sustainability: Pt. I, System Design," in *Procedia Manufacturing*, Elsevier B.V., 2018, pp. 266–272. doi: 10.1016/j.promfg.2018.02.120.
- [44] Y. Yildiz and M. Nalbant, "A review of cryogenic cooling in machining processes," Jul. 2008. doi: 10.1016/j.ijmachtools.2008.01.008.
- [45] Teagutec turning line and New product news, "N P N N e w P r o d u c t N e w s New Modular Head and Holder for Swiss Machines," 2023. [Online]. Available: www.taegutec.com
- [46] S. Tamang and S. Aravindan, "Brazing of cBN to WC-Co by Ag-Cu-In-Ti alloy through microwave hybrid heating for cutting tool application," *Mater Lett*, vol. 254, pp. 145–148, Nov. 2019, doi: 10.1016/j.matlet.2019.07.041.
- [47] D. C. . Montgomery, *Design and analysis of experiments*. John Wiley & Sons, Inc., 2013.
- [48] S. Y. Hong and Y. Ding, "Cooling approaches and cutting temperatures in cryogenic machining of Ti-6Al-4V," 2001.
- [49] B. Stampfer, P. Golda, R. Schießl, U. Maas, and V. Schulze, "Cryogenic orthogonal turning of Ti-6Al-4V: Analysis of nitrogen supply pressure variation and subcooler usage," *International Journal of Advanced Manufacturing Technology*, vol. 111, no. 1–2, pp. 359–369, Nov. 2020, doi: 10.1007/s00170-020-06105-z.
- [50] L. Gong, Y. Su, Y. Liu, W. Zhao, A. M. Khan, and M. Jamil, "Investigation on Machinability Characteristics of Inconel 718 Alloy in Cryogenic Machining Processes," *Lubricants*, vol. 11, no. 2, Feb. 2023, doi: 10.3390/lubricants11020082.
- [51] N. Hurtado-Alonso, J. Manso-Morato, V. Revilla-Cuesta, M. Skaf, and V. Ortega-López, "Optimization of cementitious mixes through response surface method: a systematic review," Jan. 01, 2025, Springer Science and Business Media Deutschland GmbH. doi: 10.1007/s43452-024-01112-3.
- [52] M. F. Ashby *et al.*, "Materials Selection in Mechanical Design." [Online]. Available: http://books.elsevier.com
- [53] K. Tyler and H. Parnell, "Performance Indices Reference Booklet," 2022.

- [54] E. B. Fonseca *et al.*, "Fracture toughness and wear resistance of heat-treated H13 tool steel processed by laser powder bed fusion," *Addit Manuf*, vol. 78, Sep. 2023, doi: 10.1016/j.addma.2023.103862.
- [55] X. Yin *et al.*, "Micro-sized polycrystalline cubic boron nitride with properties comparable to nanocrystalline counterparts," *Ceram Int*, vol. 46, no. 7, pp. 8806–8810, May 2020, doi: 10.1016/j.ceramint.2019.12.120.
- [56] A. Shokrani, V. Dhokia, and S. T. Newman, "Environmentally conscious machining of difficult-to-machine materials with regard to cutting fluids," 2012, *Elsevier Ltd.* doi: 10.1016/j.ijmachtools.2012.02.002.
- [57] S. Dabees, S. Mirzaei, P. Kaspar, V. Holcman, and D. Sobola, "Characterization and Evaluation of Engineered Coating Techniques for Different Cutting Tools—Review," Aug. 01, 2022, *MDPI*. doi: 10.3390/ma15165633.
- [58] Y. Yuan, L. Fu, and J. Li, "Annealing effect on the mechanical properties of ultrafine WC–Co materials," *Journal of Applied Research and Technology*, vol. 15, no. 4, pp. 396–401, Aug. 2017, doi: 10.1016/j.jart.2017.03.005.
- [59] J. Wang, D. Petit, and S. Ren, "Transparent thermal insulation silica aerogels," Dec. 01, 2020, *Royal Society of Chemistry*. doi: 10.1039/d0na00655f.
- [60] Y. Sun *et al.*, "Recent Advancements in Alumina-Based High-Temperature Insulating Materials: Properties, Applications, and Future Perspectives," *High-Temperature Materials*, vol. 2, no. 1, pp. 10001–10001, 2025, doi: 10.70322/htm.2025.10001.
- [61] Z. Liu, C. Yue, X. Li, X. Liu, S. Y. Liang, and L. Wang, "Research on tool wear based on 3d fem simulation for milling process," *Journal of Manufacturing and Materials Processing*, vol. 4, no. 4, Dec. 2020, doi: 10.3390/jmmp4040121.
- [62] Lienhard, "DESIGN OF HEAT FINS: HEAT CONDUCTION, FOURIER SERIES, AND FINITE DIFFERENCE APPROXIMATION."
- [63] R. Sahu and P. Singh, "Static Analysis of Cutting Tool using Finite Element Approach," *International Research Journal of Engineering and Technology*, vol. 557, 2008, [Online]. Available: www.irjet.net
- [64] R. G. Budynas and J. K. Nisbett, "Shigley's Mechanical Engineering Design," 2015.
- [65] L. Gong, Y. Su, Y. Liu, W. Zhao, A. M. Khan, and M. Jamil, "Investigation on Machinability Characteristics of Inconel 718 Alloy in Cryogenic Machining

- Processes," *Lubricants*, vol. 11, no. 2, Feb. 2023, doi: 10.3390/lubricants11020082.
- [66] K. Bartsch, B. Bossen, W. Chaudhary, M. Landry, and D. Herzog, "Thermal Conductivity of Ti-6Al-4V in Laser Powder Bed Fusion," *Front Mech Eng*, vol. 8, Jul. 2022, doi: 10.3389/fmech.2022.830104.